universe

IMPACT FACTOR 2.813

CITESCORE 3.2

Article

Dirac Observables in the 4-Dimensional Phase Space of Ashtekar's Variables and Spherically Symmetric Loop Quantum Black Holes

Geeth Ongole, Hongchao Zhang, Tao Zhu, Anzhong Wang and Bin Wang

Special Issue

Loop Quantum Gravity: A Themed Issue in Honor of Prof. Abhay Ashtekar

Edited by

Prof. Dr. Parampreet Singh

MDPI

https://doi.org/10.3390/universe8100543

universe

MDPI

Article

Dirac Observables in the 4-Dimensional Phase Space of Ashtekar's Variables and Spherically Symmetric Loop Quantum Black Holes

Geeth Ongole [1], Hongchao Zhang [2,3], Tao Zhu [2,3], Anzhong Wang [1,*] and Bin Wang [4,5]

[1] GCAP-CASPER, Physics Department, Baylor University, Waco, TX 76798-7316, USA
[2] Institute for Theoretical Physics & Cosmology, Zhejiang University of Technology, Hangzhou 310023, China
[3] United Center for Gravitational Wave Physics (UCGWP), Zhejiang University of Technology, Hangzhou 310023, China
[4] Center for Gravitation and Cosmology, College of Physical Science and Technology, Yangzhou University, Yangzhou 225009, China
[5] Shanghai Frontier Science Center for Gravitational Wave Detection, Shanghai Jiao Tong University, Shanghai 200240, China
* Correspondence: anzhong_wang@baylor.edu

Abstract: In this paper, we study a proposal put forward recently by Bodendorfer, Mele and Münch and García-Quismondo and Marugán, in which the two polymerization parameters of spherically symmetric black hole spacetimes are the Dirac observables of the four-dimensional Ashtekar's variables. In this model, black and white hole horizons in general exist and naturally divide the spacetime into the external and internal regions. In the external region, the spacetime can be made asymptotically flat by properly choosing the dependence of the two polymerization parameters on the Ashtekar variables. Then, we find that the asymptotical behavior of the spacetime is universal, and, to the leading order, the curvature invariants are independent of the mass parameter m. For example, the Kretschmann scalar approaches zero as $K \simeq A_0 r^{-4}$ asymptotically, where A_0 is generally a non-zero constant and independent of m, and r the geometric radius of the two-spheres. In the internal region, all the physical quantities are finite, and the Schwarzschild black hole singularity is replaced by a transition surface whose radius is always finite and non-zero. The quantum gravitational effects are negligible near the black hole horizon for very massive black holes. However, the behavior of the spacetime across the transition surface is significantly different from all loop quantum black holes studied so far. In particular, the location of the maximum amplitude of the curvature scalars is displaced from the transition surface and depends on m; so does the maximum amplitude. In addition, the radius of the white hole is much smaller than that of the black hole, and its exact value sensitively depends on m, too.

Keywords: quantum black holes; singularity resolution; asymptotical behavior

Citation: Ongole, G.; Zhang, H.; Zhu, T.; Wang, A.; Wang, B. Dirac Observables in the 4-Dimensional Phase Space of Ashtekar's Variables and Spherically Symmetric Loop Quantum Black Holes. *Universe* **2022**, *8*, 543. https://doi.org/10.3390/universe8100543

Academic Editor: Etera Livine

Received: 6 September 2022
Accepted: 14 October 2022
Published: 19 October 2022

1. Introduction

Loop quantum gravity (LQG) has burgeoned in an effort to quantize gravity. It is a non-perturbative and background independent approach to canonically quantizing Einstein's general relativity (GR) [1–5]. Loop quantum cosmology (LQC) is an application of the LQG techniques by first performing the symmetry reduction of the homogeneous and isotropic spacetimes at the classical level, and then quantizing it by using the canonical Dirac quantization for systems with constraints, the so-called minisuperspace approach [6]. Singularities are one of the major predictions by GR, which appear (classically) in the very early cosmological epoch and the interior regions of black holes. Classical GR becomes invalid when such singularities appear. One usually expects that in such high curvature regimes quantum gravitational effects will take over and become dominant, whereby the singularities are smoothed out and finally replaced by regions with the Planck scale

curvatures. Because of the quantum nature of geometry in LQG, cosmological singularities can be naturally resolved in LQC models, without any additional constraints on matter fields [6]. Although the full theory is still under construction, symmetry reduced models constructed from LQG have received great attention.

Since the Schwarzschild interior is isometric to the homogeneous but anisotropic (vacuum) Kantowski–Sachs cosmological model, techniques of LQC can be used to study black hole(BH) singularities in the spherically symmetric spacetimes. In the treatment of LQC, the full quantum evolution is well approximated by quantum corrected effective equations. Similar treatment is applied to the interior of the Schwarzschild spacetime to obtain the quantum corrected Schwarzschild spacetime, which cures the black hole singularity. Recently, such works have received lot of attention [7–52].

A particular model proposed recently is the Ashtekar–Olmedo–Singh (AOS) loop quantum black hole (LQBH) [53–55], in which AOS constructed the effective Hamiltonian that governs the dynamics of spherically symmetric loop quantum black holes in the semi-classical limit. This effective Hamiltonian contains two polymerization parameters (δ_b, δ_c), characterizing the quantum gravitational effects. In some of the previous approaches, they were simply taken as constants [7,11,31,33], similar to the μ_0 scheme first introduced in LQC [6]. However, in LQC it was found [56] that the μ_0 scheme leads to large quantum geometric effects even in regions much lower than the Planck curvatures. To remand this problem, Ashtekar, Pawlowski and Singh (APS) [56] proposed that the polymerization parameter should depend on phase variables, the so-called $\bar{\mu}$ scheme [1]. It turns out that so far this is the only scheme that leads to consistent results in LQC [6].

On the other hand, in the AOS model [53–55], instead of treating (δ_b, δ_c) as arbitrary functions of the phase variables, they consider them as Dirac observables, that is, they are particular functions of the phase variables, such that along the trajectories of the effective Hamiltonian equations they become constants. Similar treatments have also been adopted in [9,14,15,23,24]. However, the AOS approach is different as they considered (δ_b, δ_c) as Dirac observables in the 8-dimensional extended phase space $\Gamma_{\rm ext}$ of the variables $\left(b, c, p_b, p_c; \delta_b, \delta_c, p_{\delta_b}, p_{\delta_c}\right)$, instead of the 4-dimensional phase space Γ of the variables (b, c, p_b, p_c). Another key feature that differentiates the AOS approach is the imposition of the minimum area condition of LQG on the plaquettes that tesselate the transition surface. This treatment helped resolve the long standing problems in LQBH such as the dependence of the system on the fiducial structure and non-negligible quantum corrections at low curvatures, to name a few.

Despite the success of the AOS model, some questions have been raised [57,58]. In particular, Bodendorfer, Mele and Münch (BMM) [59] argued that the polymerization parameters can be treated canonically as Dirac observables directly in the 4-dimensional phase space Γ, so that $\delta_i = f_i(O_i),\ (i = b, c)$, where O_i's are the two independent Dirac observables that can be constructed in the spherically symmetric spacetimes, and are given explicitly by Equation (10) below in terms of the four Ashtekar variables (b, c, p_b, p_c). Then, the corresponding dynamics of the effective Hamiltonian is different from that of AOS. More recently, García-Quismondo and Marugán (GM) [60] argued that in the BMM approach, the two polymerization parameters in general should depend on both O_b and O_c, that is, $\delta_i = f_i(O_b, O_c)$, and the BMM choice can be realized as a special case. GM also derived the corresponding dynamical equations.

In this paper, we shall study the main properties of the LQBH spacetimes resulting from the BMM/GM proposal. In particular, the paper will be organized as follows: in Section 2 we will briefly review the AOS model, so readers can clearly see the difference between the AOS and BMM/GM approaches. In Section 3, we first introduce the BMM/GM model and then restrict ourselves to the external region of the BMM/GM LQBH spacetime. By requiring that the spacetime in this region be asymptotically flat, we find that the parameter $\Omega_b\ [\equiv \omega_{bb} + \omega_{bc}]$ must be non-negative $\Omega_b \geq 0$, where $\omega_{ij} \equiv \partial f_i/\partial O_j$ [cf. Equation (60)]. This excludes the BMM choice $\delta_i = f_i(O_i)$ [59], which is also the choice made by AOS [53–55], but it must be noted that AOS did it in the extended phase space.

With this condition, we find that the asymptotical behavior of the spacetime is universal and independent of the mass parameter m for the curvature invariants [cf. Equations (72) and (88)]. In particular, the Kretschmann scalar behaves as $K \to A_0 r^{-4}$ as $r \to \infty$, where A_0 is a constant and independent of m, and r the geometric radius of the two-spheres. Similar behavior is also found in the AOS model.

In Section 4, we analyze the properties of the BMM/GM model in the internal region and find that all the physical quantities are finite, and the Schwarzschild black hole singularity is replaced by a transition surface whose radius is always finite and non-zero. However, the behavior of the spacetime across the transition surface is significantly different from all LQBHs studied previously. In particular, the curvature invariants, such as the Kretschmann scalar, achieve their maxima not at the transition surface but right after or before crossing it. Detailed investigations of the metric components reveal that this is because of the fact that now δ_is are the Dirac observables in the 4D phase space, which considerably modify the structure of the spacetime. Due to such modifications, the location of the white hole horizon is also very near to the transition surface, and the ratio of the white and black hole horizon radii is much smaller than one, and sensitively depends on the mass parameter m. Finally, in Section 5, we summarize our main conclusions.

To distinguish the AOS and BMM/GM approaches, in this paper, we shall refer them as to the *extended and canonical phase space approaches*, respectively.

Before proceeding further, we would also like to note that parts of the results presented in this paper had been reported in the APS April meeting, 9–12 April 2022, New York, as well as in the 23rd International Conference on General Relativity and Gravitation (GR23), Liyang, China, 3–8 July 2022.

2. Extended Phase Space Approach

The starting point of LQG is the introduction of the Ashtekar variables. In the spherically symmetric spacetimes, they are the metric components p_b and p_c and their moment conjugates b and c with the canonical relations

$$\{b, p_b\} = G\gamma, \quad \{c, p_c\} = 2G\gamma, \tag{1}$$

where γ is the Barbero–Immirzi parameter and G is the Newtonian gravitational constant.

In terms of p_b and p_c, the four-dimensional spacetime line element takes the form,

$$ds^2 = -N^2 dT^2 + \frac{p_b^2}{|p_c| L_o^2} dx^2 + |p_c| d\Omega^2, \tag{2}$$

where N is the lapse function, and L_o is a constant, denoting the length of the fiducial cell in the x-direction with $x \in (0, L_o)$, and $d\Omega^2 \equiv d\theta^2 + \sin^2\theta d\phi^2$ with θ and ϕ being the two angular coordinates defined on the two spheres $T, x =$ Constant.

In the internal region of a classical black hole, (N, p_b, p_c) are all functions of T only (so are b and c), and the corresponding spacetimes are of the Kantowski–Sachs cosmological model, which allows one to apply LQC techniques to such homogeneous but anisotropic spacetimes. As a result, the internal region of the Schwarzschild has been extensively studied in the framework of LQC.

On the other hand, in the external region, the coordinates T and x exchange their rules, and the spacetime becomes static. However, such changes can be also carried out by the replacement $N \to iN$ and $p_b \to ip_b$, as shown explicitly below, while keeping the dependence of the Ashtekar variables still only on T.

With the above in mind, we can see that in general the metric (2) has the gauge freedom,

$$T' = T'(T), \quad x' = \alpha x + x_0, \tag{3}$$

in both external and internal regions, where $T'(T)$ is an arbitrary function of T only, and α and t_0 are real constants. To see the AOS approach more clearly, let us consider the AOS effective Hamiltonian inside and outside the LQBH, separately.

2.1. AOS Internal Solution

With the gauge freedom of (3), AOS chose $T'(T)$ so that:

$$N = \frac{\gamma\delta_b \,\mathrm{sgn}(p_c)\sqrt{|p_c|}}{\sin(\delta_b b)}. \tag{4}$$

Then, the effective Hamiltonian in the interior of LQBHs reads [53–55]:

$$H_{\rm eff} = -\tfrac{1}{2G\gamma}\left[\; 2\tfrac{\sin(\delta_c c)}{\delta_c}|p_c| + \left(\tfrac{\sin(\delta_b b)}{\delta_b} + \tfrac{\gamma^2\delta_b}{\sin(\delta_b b)}\right)p_b\right], \tag{5}$$

where δ_b and δ_c are two Dirac observables, appearing in the polymerizations,

$$b \to \frac{\sin(\delta_b b)}{\delta_b}, \quad c \to \frac{\sin(\delta_c c)}{\delta_b}. \tag{6}$$

That is, replacing b and c by Equation (6) in the classical Hamiltonian,

$$H_{\rm cl} = -\frac{1}{2G\gamma}\left[2c|p_c| + \left(b + \frac{\gamma^2}{b}\right)p_b\right], \tag{7}$$

whereby the effective Hamiltonian (5) is obtained, provided that the classical lapse function is chosen as:

$$N_{\rm cl} = \frac{\gamma\,\mathrm{sgn}(p_c)\sqrt{|p_c|}}{b}. \tag{8}$$

To fix δ_b and δ_c, AOS first noticed that the above effective Hamiltonian can be written as:

$$H_{\rm eff} = \frac{L_o}{G}(O_b - O_c), \tag{9}$$

where

$$O_b \equiv -\frac{p_b}{2\gamma L_o}\left(\frac{\sin(\delta_b b)}{\delta_b} + \frac{\gamma^2\delta_b}{\sin(\delta_b b)}\right), \tag{10}$$

$$O_c \equiv \frac{|p_c|}{\gamma L_o}\frac{\sin(\delta_c c)}{\delta_c}, \tag{11}$$

are two Dirac observables. Then, AOS proceeded as follows:

- First extend the 4-dimensional (4D) phase space Γ spanned by $(b, c; p_b, p_c)$ to 8-dimensional (8D) phase space $\Gamma_{\rm ext}$ spanned by $\left(b, c, \delta_b, \delta_c; p_b, p_c, p_{\delta_b}, p_{\delta_c}\right)$. In $\Gamma_{\rm ext}$ the variables δ_b and δ_c are independent, so they are in particular not functions of (b, c, p_b, p_c) and instead Poisson commute with all of them;
- Lift $H_{\rm eff}$ given by Equation (5) to $\Gamma_{\rm ext}$, and then consider its Hamiltonian flow. Since O_b and O_c are the Dirac observables of this flow, the following choice can be made

$$\delta_b = \delta_b(O_b), \quad \delta_c = \delta_c(O_c), \tag{12}$$

  so that (δ_b, δ_c) are also the Dirac observables;
- Introduce these dependences as two new first-class constraints:

$$\begin{aligned} \Phi_b &\equiv O_b - F_b(\delta_b) \simeq 0, \\ \Phi_c &\equiv O_c - F_c(\delta_c) \simeq 0, \end{aligned} \tag{13}$$

so that the four-dimensional reduced $\hat{\Gamma}$ corresponding to these constraints is symplectomorphic to the original phase space Γ. Since O_b and O_c are the Dirac observables, Equation (13) implies:

$$\delta_b = F_b^{-1}(O_b), \quad \delta_c = F_c^{-1}(O_c), \tag{14}$$

are also constants on the trajectories of the effective Hamiltonian $H_{\rm eff}$ given by Equation (5).

- To fix δ_b and δ_c, AOS assumed that at the transition surface, (where $T = \mathcal{T}$), the physical areas of the (x, θ)- and (θ, ϕ)-planes are respectively equal to the minimal area Δ [53]

$$2\pi\delta_c\delta_b|p_b(\mathcal{T})| = \Delta, \tag{15}$$
$$4\pi\delta_b^2 p_c(\mathcal{T}) = \Delta. \tag{16}$$

With all the above, AOS found that the corresponding Hamilton equations are given by:

$$\dot{b} = -\frac{1}{2}\left(\frac{\sin(\delta_b b)}{\delta_b} + \frac{\gamma^2\delta_b}{\sin(\delta_b b)}\right), \tag{17}$$
$$\dot{p}_b = \frac{1}{2}p_b\cos(\delta_b b)\left(1 - \frac{\gamma^2\delta_b^2}{\sin^2(\delta_b b)}\right), \tag{18}$$

and

$$\dot{c} = -2\frac{\sin(\delta_c c)}{\delta_c}, \tag{19}$$
$$\dot{p}_c = 2p_c\cos(\delta_c c). \tag{20}$$

It is remarkable to note that, in the above equations, no cross terms exists between the equations for (b, p_b) and the ones for (c, p_c). As a result, we can solve the two sets of equations independently, and the corresponding solutions are given by [52,53]:

$$\cos(\delta_b b) = b_o\frac{1 + b_o\tanh\left(\frac{b_o T}{2}\right)}{b_o + \tanh\left(\frac{b_o T}{2}\right)} = b_o\frac{b_+ e^{b_o T} - b_-}{b_+ e^{b_o T} + b_-},$$
$$p_b = -\frac{mL_o}{2b_o^2}\left(b_+ + b_- e^{-b_o T}\right)\mathcal{A}, \tag{21}$$
$$\sin(\delta_c c) = \frac{2a_o e^{2T}}{a_o^2 + e^{4T}},$$
$$p_c = 4m^2\left(a_o^2 + e^{4T}\right)e^{-2T}, \tag{22}$$

where

$$\mathcal{A} \equiv \left[2\left(b_o^2 + 1\right)e^{b_o T} - b_-^2 - b_+^2 e^{2b_o T}\right]^{1/2},$$
$$a_o \equiv \frac{\gamma\delta_c L_o}{8m}, \quad b_o \equiv \left(1 + \gamma^2\delta_b^2\right)^{1/2},$$
$$b_\pm \equiv b_o \pm 1, \tag{23}$$

with

$$\delta_b b \in (0, \pi), \quad \delta_c c \in (0, \pi), \quad p_b \leq 0, \quad p_c \geq 0, \quad -\infty < T < 0. \tag{24}$$

The parameter m is an integration constant, related to the mass parameter of the AOS solution. From the above solution, it can be shown that the two Dirac observables on-shell are given by:

$$O_b = m = O_c. \tag{25}$$

In the large mass limit, $m \gg m_p$, from Equations (15) and (16) AOS found that

$$\delta_b = \left(\frac{\sqrt{\Delta}}{\sqrt{2\pi}\gamma^2 m}\right)^{\frac{1}{3}}, \quad L_0\delta_c = \frac{1}{2}\left(\frac{\gamma\Delta^2}{4\pi^2 m}\right)^{\frac{1}{3}}, \tag{26}$$

where m_p denotes the Planck mass.

It should be noted that in [53] two solutions for c were given, and here in this paper we only consider the one with "+" sign, as physically they describe the same spacetime.

From Equation (22), it can be seen that the transition surface is located at $\partial p_c(T)/\partial T|_{T=\mathcal{T}} = 0$, which yields:

$$\mathcal{T} = \frac{1}{2}\ln\left(\frac{\gamma\delta_c L_o}{8m}\right) < 0. \tag{27}$$

There also exist two horizons, located respectively at:

$$T_{\rm BH} = 0, \quad T_{\rm WH} = -\frac{2}{b_o}\ln\left(\frac{b_o+1}{b_o-1}\right), \tag{28}$$

at which we have $\mathcal{A}(T) = 0$, where $T = T_{\rm BH}$ is the location of the black hole horizon, while $T = T_{\rm WH}$ is the location of the white hole. In the region $\mathcal{T} < T < 0$, the 2-spheres are all trapped, while in the one $T_{\rm WH} < T < \mathcal{T}$, they are all anti-trapped. Therefore, the region $\mathcal{T} < T < 0$ behaves like the BH interior, while the one $T_{\rm WH} < T < \mathcal{T}$ behaves like the WH interior, denoted, respectively, by Region B and Region W in Figure 1. This explains the reason why we call them the black hole and white hole regions, although the geometric radius $\sqrt{p_c}$ of the two-sphere (T, x = Const) is always finite and non-zero, so spacetime singularities never appear.

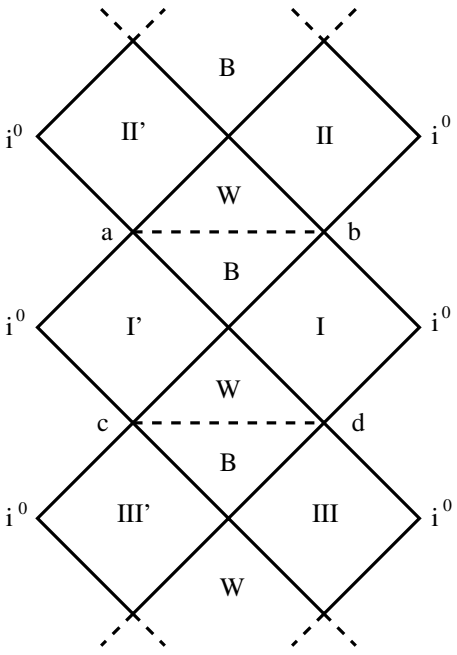

Figure 1. The Penrose diagram for the AOS LQBH. The dashed horizontal lines *ab* and *cd* represent the transition surfaces (throats), and the regions marked with B is the BH interior, and the regions marked with W is the WH interior, but there are no spacetime singularities, so the extensions are infinite along the vertical line in both directions. Regions marked with I, I', II, II', III, and III' are asymptotically flat regions but with a falling rate slower than that of the Schwarzschild black hole [55].

Finally, we note that in this region the lapse function reads:

$$N = \frac{\gamma\delta_b \,\mathrm{sgn}(p_c)|p_c|^{1/2}}{\sin(\delta_b b)} = \frac{2m}{\mathcal{A}}\left(b_+ e^{b_o T} + b_-\right)\left(a_o^2 e^{-2T} + e^{2T}\right)^{1/2}, \tag{29}$$

where $\mathcal{A}$ is given in Equation (23).

2.2. AOS External Solution

At the two horizons (28), we have $\mathcal{A}(T) = 0$, and the metric becomes singular, so extensions beyond these surfaces are needed in order to obtain a geodesically complete spacetime. AOS showed that such extensions can be obtained from (5) by the following replacements:

$$b \to ib, \quad p_b \to ip_b, \quad c \to c, \quad p_c \to p_c, \tag{30}$$

for which the canonical relations (1) now become:

$$\{b, p_b\} = -G\gamma, \quad \{c, p_c\} = 2G\gamma, \tag{31}$$

while the effective Hamiltonian in the external space of the LQBH is given by:

$$H_{\rm eff}^{\rm ext} = -\frac{1}{2G\gamma}\left[2\frac{\sin(\delta_c c)}{\delta_c}p_c - \left(\frac{\sinh(\delta_b b)}{\delta_b} - \frac{\gamma^2\delta_b}{\sinh(\delta_b b)}\right)p_b\right] = \frac{L_o}{G}(O_b - O_c), \tag{32}$$

but now with:

$$O_b \equiv \frac{p_b}{2\gamma L_o}\left(\frac{\sinh(\delta_b b)}{\delta_b} - \frac{\gamma^2\delta_b}{\sinh(\delta_b b)}\right), \tag{33}$$

$$O_c \equiv \frac{p_c}{\gamma L_o}\frac{\sin(\delta_c c)}{\delta_c}, \tag{34}$$

which can be obtained directly from Equations (10) and (11) with the replacement (30). Then, the corresponding Hamilton equations for (c, p_c) are still given by Equations (19) and (20), while the ones for (b, p_b) now are replaced by:

$$\dot{b} = -\frac{1}{2}\left(\frac{\sinh(\delta_b b)}{\delta_b} - \frac{\gamma^2\delta_b}{\sinh(\delta_b b)}\right), \tag{35}$$

$$\dot{p}_b = \frac{1}{2}p_b\cosh(\delta_b b)\left(1 + \frac{\gamma^2\delta_b^2}{\sinh^2(\delta_b b)}\right). \tag{36}$$

Then, the corresponding solutions of the Hamilton equations are given by:

$$\begin{aligned}
\cosh(\delta_b b) &= b_o\frac{1 + b_o\tanh\left(\frac{b_o T}{2}\right)}{b_o + \tanh\left(\frac{b_o T}{2}\right)}, \\
p_b &= -2m\gamma L_o\delta_b\frac{\sinh(\delta_b b)}{\gamma^2\delta_b^2 - \sinh^2(\delta_b b)} = -\frac{mL_o}{2b_o^2}\left(b_+ + b_- e^{-b_o T}\right)\mathcal{A}, \qquad (37) \\
\sin(\delta_c c) &= \frac{2a_o e^{2T}}{a_o^2 + e^{4T}}, \\
p_c &= 4m^2\left(e^{2T} + a_o^2 e^{-2T}\right), \qquad (38)
\end{aligned}$$

but now with

$$\mathcal{A} \equiv \left[b_-^2 + b_+^2 e^{2b_o T} - 2\left(b_o^2 + 1\right)e^{b_o T}\right]^{1/2}, \tag{39}$$

which can be obtained from Equation (23) by the replacement $\mathcal{A} \to i\mathcal{A}$ (or $\mathcal{A}^2 \to -\mathcal{A}^2$), so that $g_{xx} \to -g_{xx}$, and the coordinate x now becomes timelike in the external region ($T > 0$) of the black hole horizon, located at $T = 0$. It can be shown that for the above solution, we have $O_b = m = O_c$, which shows clearly that O_b and O_c defined by Equations (33) and (34) are two Dirac observables.

We also note that the replacement of Equation (30) leads to:

$$N^2 = -\frac{\gamma^2\delta_b^2|p_c|}{\sinh^2(\delta_b b)} = -\frac{4m^2}{\mathcal{A}^2}\left(b_+ e^{b_o T} + b_-\right)^2\left(a_o^2 e^{-2T} + e^{2T}\right), \tag{40}$$

so that, in terms of N, p_b and p_c, the metric now takes the form [53]:

$$\begin{aligned} ds^2 &= -N^2dT^2 - \frac{p_b^2}{|p_c|L_o^2}dx^2 + |p_c|d\Omega^2 \\ &= -\frac{p_b^2}{|p_c|L_o^2}dx^2 + \frac{\gamma^2\delta_b^2|p_c|}{\sinh^2(\delta_b b)}dT^2 + |p_c|d\Omega^2, \end{aligned} \tag{41}$$

which shows clearly that now T is spacelike, while x becomes timelike, so the spacetime outside of the LQBH is static.

In addition, AOS showed that the two metrics (2) and (41) are analytically connected to each other across the two horizons, and as a result, the extensions are unique. The global structure of the spacetime is given by the Penrose diagram of Figure 1, from which we can see that the extensions along the vertical direction are infinite, quite similar to the charged spherically symmetric Reissner–Nordström solutions [61], but without spacetime singularities, as now the geometric radius $\sqrt{p_c}$ never becomes zero.

Before proceeding to the next section, we also note that technically the AOS extended space approach can be realized directly by taking δ_b and δ_c to be constants in the phase space of (b, c, p_b, p_c), and then impose the conditions (15) and (16), as by definition, constants over the whole phase space are also Dirac observables.

3. Canonical Phase Space Approach

Instead of extending the 4D physical phase space to 8D phase space, and then considering δ_b and δ_c as the Dirac observables of the extended phase space, Bodendorfer, Mele, and Münch (BMM) pointed out [59] that they can be considered directly as the Dirac observables in the 4D physical phase space of (b, c, p_b, p_c), as those given by Equation (12). Lately, García-Quismondo and Marugán argued [60] that δ_b and δ_c should in general depend on both of the two Dirac observables O_b and O_c,

$$\delta_i = f_i(O_b, O_c), \ (i = b, c), \tag{42}$$

while Equation (12) only represents a particular choice of the general case. Equation (42) shows clearly that now δ_b and δ_c all depend on the four variables, (b, c, p_b, p_c), through Equations (10) and (11) [or Equations (33) and (34) when outside of the LQBH]. Then, the corresponding Hamilton equations are given by [60]:

$$\partial_T i = C_{ij}\left[s_i\frac{L_o}{G}\{i, p_i\}\frac{\partial O_i}{\partial p_i}\right], \tag{43}$$

$$\partial_T p_i = C_{ij}\left[-s_i\frac{L_o}{G}\{i, p_i\}\frac{\partial O_i}{\partial i}\right], \tag{44}$$

where $i, j = b, c$, $i \neq j$, $s_b = 1$, $s_c = -1$, and

$$C_{ij} \equiv \frac{1 - \Delta_{jj} - \Delta_{ji}}{(1 - \Delta_{ii})(1 - \Delta_{jj}) - \Delta_{ij}\Delta_{ji}}, \tag{45}$$

$$\Delta_{ij} \equiv \frac{\partial O_i}{\partial \delta_i}\frac{\partial f_i}{\partial O_j}. \tag{46}$$

It is interesting to note that, introducing two new variables, t_i, $(i = b, c)$, via the relations:

$$dt_i \equiv C_{ij} dT, \ (i \neq j), \tag{47}$$

Equations (43) and (44) take the forms,

$$\partial_{t_i} i = s_i \frac{L_o}{G}\{i, p_i\}\frac{\partial O_i}{\partial p_i}, \tag{48}$$

$$\partial_{t_i} p_i = -s_i \frac{L_o}{G}\{i, p_i\}\frac{\partial O_i}{\partial i}, \tag{49}$$

which will lead to the same Hamilton equations as those given by AOS, if we replace T by t_b in the equations for b and p_b, and T by t_c in the equations for c and p_c, as first noted in [60]. This observation will significantly simplify our following discussions.

To proceed further, in the rest of this section, let us consider the above equations only in the external region, while the ones in the internal region will be considered in the next section.

3.1. Dynamics of the external LQBH Spacetimes

In the external region, the Hamilton equations take the form

$$\frac{db}{dt_b} = -\frac{1}{2}\left(\frac{\sinh(\delta_b b)}{\delta_b} - \frac{\gamma^2 \delta_b}{\sinh(\delta_b b)}\right), \tag{50}$$

$$\frac{dp_b}{dt_b} = \frac{1}{2} p_b \cosh(\delta_b b)\left(1 + \frac{\gamma^2 \delta_b^2}{\sinh^2(\delta_b b)}\right), \tag{51}$$

for (b, p_b), and

$$\frac{dc}{dt_c} = -2\frac{\sin(\delta_c c)}{\delta_c}, \tag{52}$$

$$\frac{dp_c}{dt_c} = 2 p_c \cos(\delta_c c), \tag{53}$$

for (c, p_c). Then, the corresponding solutions for b and p_b will be given by Equations (37) and (39) by simply replacing T by t_b, that is,

$$\cosh(\delta_b b) = b_o \frac{1 + b_o \tanh\left(\frac{b_o t_b}{2}\right)}{b_o + \tanh\left(\frac{b_o t_b}{2}\right)},$$

$$p_b = -\frac{m L_o}{2 b_o^2}\left(b_+ + b_- e^{-b_o t_b}\right)\mathcal{A},$$

$$\mathcal{A} \equiv \left[b_-^2 + b_+^2 e^{2 b_o t_b} - 2\left(b_o^2 + 1\right) e^{b_o t_b}\right]^{1/2}, \tag{54}$$

while the solutions for c and p_c will be given by Equation (38) with the replacement T by t_c, i.e.,

$$\sin(\delta_c c) = \frac{2 a_o e^{2 t_c}}{a_o^2 + e^{4 t_c}}, \quad p_c = 4 m^2\left(e^{2 t_c} + a_o^2 e^{-2 t_c}\right). \tag{55}$$

The relation between t_b and t_c is given by Equation (47), from which we find that

$$dt_c = \frac{C_{cb}}{C_{bc}} dt_b. \tag{56}$$

To study the above relation, let us first note that Equations (33) and (34) lead to:

$$\begin{aligned}
\frac{\partial O_b}{\partial \delta_b} &= \frac{p_b}{2\gamma L_o \delta_b^2}\left(1 + \frac{\gamma^2\delta_b^2}{\sinh^2(\delta_b b)}\right)\left[(\delta_b b)\cosh(\delta_b b) - \sinh(\delta_b b)\right], \\
\frac{\partial O_c}{\partial \delta_c} &= \frac{p_c}{\gamma L_o \delta_c^2}\left[(\delta_c c)\cos(\delta_c c) - \sin(\delta_c c)\right].
\end{aligned} \tag{57}$$

Then, we find that:

$$\begin{aligned}
C_{bc} &= \frac{1}{\mathcal{D}}\left(1 - \Omega_c \frac{\partial O_c}{\partial \delta_c}\right) \\
&= \frac{1}{\mathcal{D}}\left\{1 - \frac{\Omega_c p_c}{\gamma L_o \delta_c^2}\left[(\delta_c c)\cos(\delta_c c) - \sin(\delta_c c)\right]\right\}, \\
C_{cb} &= \frac{1}{\mathcal{D}}\left(1 - \Omega_b \frac{\partial O_b}{\partial \delta_b}\right) \\
&= \frac{1}{\mathcal{D}}\left\{1 - \frac{\Omega_b p_b}{2\gamma L_0 \delta_b^2}\left(1 + \frac{\gamma^2\delta_b^2}{\sinh^2(\delta_b b)}\right)\left[(\delta_b b)\cosh(\delta_b b) - \sinh(\delta_b b)\right]\right\},
\end{aligned} \tag{58}$$

where

$$\begin{aligned}
\mathcal{D} &\equiv 1 - \omega_{cc}\frac{\partial O_c}{\partial \delta_c} - \omega_{bb}\frac{\partial O_b}{\partial \delta_b} + (\omega_{bb}\omega_{cc} - \omega_{bc}\omega_{cb})\frac{\partial O_b}{\partial \delta_b}\frac{\partial O_c}{\partial \delta_c} \\
&= 1 - \frac{\omega_{cc} p_c}{\gamma L_o \delta_c^2}\left[(\delta_c c)\cos(\delta_c c) - \sin(\delta_c c)\right] \\
&\quad - \frac{\omega_{bb} p_b}{2\gamma L_0 \delta_b^2}\left(1 + \frac{\gamma^2\delta_b^2}{\sinh^2(\delta_b b)}\right)\left[(\delta_b b)\cosh(\delta_b b) - \sinh(\delta_b b)\right] \\
&\quad + \frac{\omega_{bb}\omega_{cc} - \omega_{bc}\omega_{cb}}{2\gamma^2 L_o^2 \delta_b^2 \delta_c^2} p_b p_c \left(1 + \frac{\gamma^2\delta_b^2}{\sinh^2(\delta_b b)}\right) \\
&\quad \times \left[(\delta_c c)\cos(\delta_c c) - \sin(\delta_c c)\right]\left[(\delta_b b)\cosh(\delta_b b) - \sinh(\delta_b b)\right],
\end{aligned} \tag{59}$$

$$\omega_{ij} \equiv \frac{\partial f_i}{\partial O_j}, \quad \Omega_c \equiv \omega_{cc} + \omega_{cb}, \quad \Omega_b \equiv \omega_{bb} + \omega_{bc}. \tag{60}$$

It should be noted that the numerator of C_{bc} is a function of t_c and the one of C_{cb} is a function of t_b, where t_b and t_c are related one to the other through Equation (56). In particular, for $t_b, t_c \gg 1$, from Equation (56), we find:

$$t_c - 2\beta m^2 a_o^3 + \mathcal{O}\left(e^{-4t_c}\right) = (1+\alpha_2)t_b + \frac{\alpha_1}{b_o}e^{b_o t_b} + \frac{\alpha_3}{2b_o} + \mathcal{O}\left(e^{-b_o t_b}\right), \ (t_b, t_c \gg 1), \tag{61}$$

where

$$\begin{aligned}
\alpha_1 &= \frac{m(b_o+1)^2}{2\gamma b_o^2 \delta_b^2}\left(b_o \cosh^{-1} b_o - \gamma\delta_b\right)\Omega_b, \\
\alpha_2 &= -\frac{m\gamma^2\delta_b}{\gamma^2\delta_b^2 + 1}\Omega_b,
\end{aligned} \tag{62}$$

β and α_3 are other constants, and their explicit expressions will not be given here, as they will not affect our following discussions.

It is interesting to note that for the BMM choice, $f_i = f_i(O_i)$ [cf. Equation (13)], and δ_i given by Equation (26) together with the fact that on-shell we have $O_b = m = O_c$, we find that:

$$\omega_{bb}^{\rm BMM} = -\frac{\delta_b}{3m}, \quad \omega_{cc}^{\rm BMM} = -\frac{\delta_c}{3m}, \quad \omega_{bc}^{\rm BMM} = \omega_{cb}^{\rm BMM} = 0,$$
$$\Omega_b^{\rm BMM} = -\frac{\delta_b}{3m}, \quad \Omega_c^{\rm BMM} = -\frac{\delta_c}{3m}. \tag{63}$$

To study the external spacetimes further, in the following let us consider the two cases, $\alpha_1 = 0$ and $\alpha_1 \neq 0$, separately.

3.2. External Spacetimes with $\alpha_1 \neq 0$

If $\alpha_1 \neq 0$, from Equation (61) we find that:

$$t_c \approx \frac{\alpha_1}{b_o} e^{b_o t_b}. \tag{64}$$

Then, from Equation (47) we find that $dT = dt_b/C_{bc}$, and in terms of t_b the metric (41) becomes:

$$ds^2 = -\frac{p_b^2}{|p_c| L_o^2} dx^2 + \frac{\gamma^2 |p_c| \delta_b^2}{\sinh^2(\delta_b b) C_{bc}^2} dt_b^2 + |p_c| \left(d\theta^2 + \sin^2\theta d\phi^2 \right), \tag{65}$$

where C_{bc} is given by Equation (58), and

$$\begin{aligned}
g_{xx} &\equiv \frac{p_b^2}{|p_c| L_o^2} \simeq \left(c_1 e^{2b_o t_b} + c_2 e^{b_o t_b} + c_3 + \cdots \right) \exp\left(-\frac{2\alpha_1}{b_o} e^{b_o t_b} \right), \\
g_{t_b t_b} &\equiv \frac{\gamma^2 |p_c| \delta_b^2}{\sinh^2(\delta_b b) C_{bc}^2} \simeq \left(d_1 e^{2b_o t_b} + d_2 e^{b_o t_b} + d_3 + \cdots \right) \exp\left(\frac{2\alpha_1}{b_o} e^{b_o t_b} \right), \\
g_{\theta\theta} &\equiv |p_c| \simeq 4m^2 \exp\left(\frac{2\alpha_1}{b_o} e^{b_o t_b} \right),
\end{aligned} \tag{66}$$

where (c_i, d_i) are constants defined as:

$$\begin{aligned}
c_1 &\equiv \frac{(b_o+1)^4}{16 b_o^4}, \quad c_2 \equiv -\frac{(b_o+1)^2}{4 b_o^4}, \quad c_3 \equiv -\frac{\gamma^2 \delta_b^2 (\gamma^2 \delta_b^2 + 4)}{8 b_o^4}, \\
d_1 &\equiv \frac{\omega_{bb}^2 f^2 m^4}{\gamma^2 \delta_b^4 b_o^4} (b_o+1)^4, \quad d_2 \equiv \frac{4\omega_{bb} f m^3}{\gamma^2 b_o^4 \delta_b^4} (b_o+1)^2 \left\{ \gamma b_o^2 \delta_b^2 - m\omega_{bb} \left(\gamma^3 \delta_b^3 - b_o^2 f \right) \right\}, \\
d_3 &\equiv 2m^2 \left(\frac{m\omega_{bb}}{\gamma^2 \delta_b^4 b_o^4} \left(m\omega_{bb} \left(2\gamma^6 \delta_b^6 + f^2 \left(\gamma^4 \delta_b^4 + 4\gamma^2 \delta_b^2 \left(b_o^2 + 1 \right) \right. \right. \right. \right. \\
&\quad \left. \left. \left. \left. + 8 b_o^2 + 2 \right) + 2\gamma^3 f \delta_b^3 \left(1 - 4 b_o^2 \right) \right) + 8\gamma f \delta_b^2 b_o^4 - 4\gamma^4 \delta_b^5 b_o^2 \right) + 2 \right),
\end{aligned} \tag{67}$$

with

$$\begin{aligned}
f(\gamma\delta_b) &\equiv b_o \cosh^{-1} b_o - \gamma\delta_b = b_o \ln(b_o + \gamma\delta_b) - \gamma\delta_b \\
&= \frac{1}{3}\gamma^3 \delta_b^3 + \mathcal{O}\left(\gamma^5 \delta_b^5 \right),
\end{aligned} \tag{68}$$

which is always non-zero for $\gamma\delta_b > 0$, as shown in Figure 2. The function $f(\gamma\delta_b)$ defined above must not be confused with the Dirac observables $f_i(O_b, O_c)$ $(i = b, c)$ introduced in Equation (42).

From the above expressions, it is clear that α_1 must be positive in order to have the spacetime asymptotically flat as $t_b \gg 1$. This is also consistent with Equation (64), as we

assumed that $t_b,\ t_c \gg 1$ asymptotically. Therefore, in the rest of this subsection we assume $\alpha_1 > 0$, which requires:

$$\Omega_b > 0. \tag{69}$$

It is interesting to note that, corresponding to the BMM choices of $f_i = f_i(O_i)$ and δ_i given by Equation (26), we have:

$$\Omega_b^{\rm BMM} = -\frac{\delta_b}{3m} < 0, \tag{70}$$

as given in Equation (63). Therefore, the BMM choices cannot be realized in this case.

It is also interesting to note that the spacetimes described by Equations (65)–(68) actually have similar asymptotic behavior as the AOS solution does, although the two metrics, given respectively by Equations (65) and (41), look quite different. To show this claim, let us first introduce a new spacelike coordinate ξ via the relation, $\xi = e^{b_o t_b}$, and then we find that the metric (65) becomes

$$\begin{aligned} ds^2 \ \simeq\ & -\Big(c_1\xi^2 + c_2\xi + c_3 + \cdots\Big)e^{-\alpha_0\xi}dT^2 + \left(d_1 + \frac{d_2}{\xi} + \frac{d_3}{\xi^2} + \cdots\right)e^{\alpha_0\xi}\frac{d\xi^2}{b_o^2} \\ & + 4m^2e^{\alpha_0\xi}\Big(d\theta^2 + \sin^2\theta d\phi^2\Big), \end{aligned} \tag{71}$$

where $T \equiv x$ and $\alpha_0 \equiv 2\alpha_1/b_o > 0$. Then, the corresponding curvature invariants of the above metric are given by:

$$\begin{aligned} g^{\mu\nu}R_{\mu\nu} \simeq\ & \left(\frac{2m}{r}\right)^2\left[\frac{1}{2}\left(\frac{1}{m^2} - \frac{b_o^2\alpha_0^2}{d_1}\right) + \frac{b_o^2\alpha_0(2d_1 + d_2\alpha_0)}{2d_1^2\xi} \right.\\ & \left. + \mathcal{O}\left(\frac{1}{\xi^2}\right)\right], \\ R^{\mu\nu}R_{\mu\nu} \simeq\ & \left(\frac{2m}{r}\right)^4\left[\frac{1}{8}\left(\frac{1}{m^4} + \frac{2b_o^4\alpha_0^4}{d_1^2}\right)\right.\\ & \left. - \frac{b_o^2\alpha_0(d_1^2 + 3b_o^2d_1m^2\alpha_0^2 + b_o^2d_2m^2\alpha_0^3)}{2(d_1^3m^2)\xi} + \mathcal{O}\left(\frac{1}{\xi^2}\right)\right], \\ R^{\mu\nu\alpha\beta}R_{\mu\nu\alpha\beta} \simeq\ & \left(\frac{2m}{r}\right)^4\left[\frac{d_1^2 - 2b_o^2d_1m^2\alpha_0^2 + 7b_o^4m^4\alpha_0^4}{4d_1^2m^4}\right.\\ & \left. + \frac{b_o^2\alpha_0^2(d_1d_2 - b_o^2m^2\alpha_0(16d_1 + 7d_2\alpha_0))}{2d_1^3m^2\xi} + \mathcal{O}\left(\frac{1}{\xi^2}\right)\right], \\ C^{\mu\nu\alpha\beta}C_{\mu\nu\alpha\beta} \simeq\ & \left(\frac{2m}{r}\right)^4\left[\frac{(d_1 - 4b_o^2m^2\alpha_0^2)^2}{12d_1^2m^4}\right.\\ & \left. + \frac{2b_o^2\alpha_0(2d_1 + d_2\alpha_0)(d_1 - 4b_o^2m^2\alpha_0^2)}{3d_1^3m^2\xi} + \mathcal{O}\left(\frac{1}{\xi^2}\right)\right], \end{aligned} \tag{72}$$

where $r\Big(\equiv 2me^{\alpha_0\xi/2}\Big)$ is the geometric radius of the two spheres $\xi,\ T =$ constant. Comparing the above with the ones presented in [55], we can see that now the metric approaches asymptotically to the Minkowski spacetime as r^{-4}, which is the same as that of the AOS solution.

It is also remarkable to note that for the AOS choices of δ_b and δ_c given by Equation (26), we find that $\alpha_1 \propto m^{2/3}$ and $d_1 \propto m^{10/3}$. Then, the above expressions show that they are all independent of m asymptotically. In particular, we have:

$$R^{\mu\nu\alpha\beta}R_{\mu\nu\alpha\beta} \simeq \frac{A_0}{r^4} + \mathcal{O}\left(\frac{1}{r^4\xi}\right), \tag{73}$$

where $\tilde{\zeta} = \frac{2}{\alpha_0}\ln\left(\frac{r}{2m}\right)$, and A_0 is independent of m given by:

$$A_0 \equiv \frac{28\Omega_b^4}{\omega_{bb}^4} - \frac{8\Omega_b^2}{\omega_{bb}^2} + 4. \tag{74}$$

This is sharply in contrast to the relativistic case, in which the Kretschmann scalar is given by:

$$R^{\mu\nu\alpha\beta}R_{\mu\nu\alpha\beta}\Big|_{\rm GR} = \frac{48m^2}{r^6}. \tag{75}$$

It is also very interesting to note that the leading order of the Kretschmann scalar of the AOS solution also behaves like r^{-4} as $r \to \infty$ [57]. In the current case, even the Dirac observables f_i are chosen so that A_0 given by Equation (74) is zero, the next leading order is $\mathcal{O}\left(\frac{1}{r^4\tilde{\zeta}}\right)$, which approaches zero still not as fast as r^{-6}. In fact, it is even slower than r^{-5}.

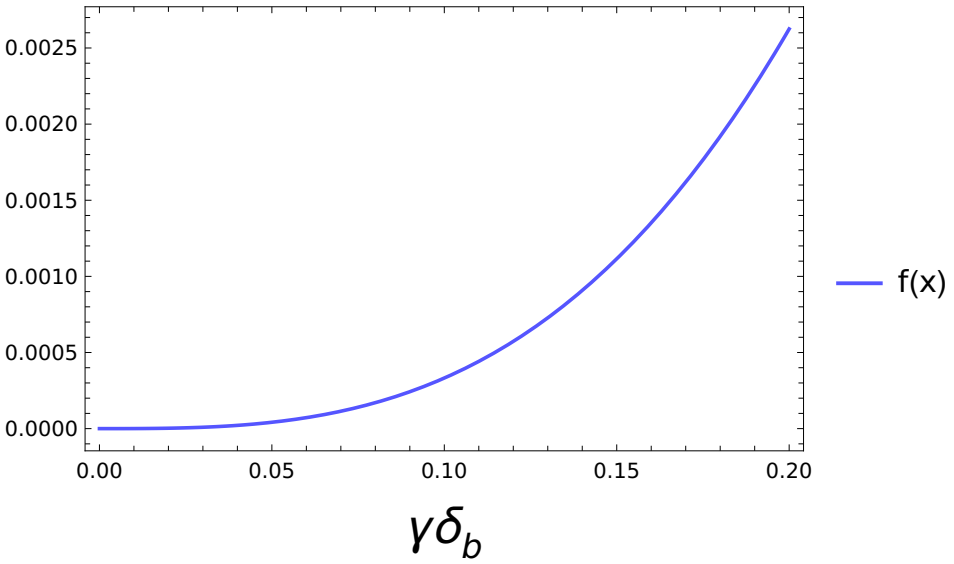

Figure 2. The function $f(x)$ defined by Equation (68) vs. $x \equiv \gamma\delta_b$.

To understand the solutions further, we first note that to the leading order the metric takes the form:

$$ds^2 \simeq -\frac{c_1 b_o^2}{\alpha_1^2}\left(\frac{\ln\left(\frac{r}{2m}\right)}{\frac{r}{2m}}\right)^2 dT^2 + \frac{d_1}{4m^2\alpha_1^2}dr^2 + r^2 d\Omega^2, \tag{76}$$

for $r \gg 2m$. On the other hand, the AOS solution takes the asymptotic form [57]:

$$ds^2_{\rm AOS} \simeq -r^{2(b_o-1)}dT^2 + dr^2 + r^2 d\Omega^2, \tag{77}$$

which is identical to the global monopole solution found in a completely different content [62]. Then, the corresponding effective energy-momentum tensor is given by:

$$T_{\nu\nu} = u_\mu u_\nu \rho + p_r r_\mu r_\nu + p_\perp\left(\theta_\mu\theta_\nu + \phi_\mu\phi_\nu\right), \tag{78}$$

where u_μ denotes the unit timelike vector along T-direction, and r_μ, θ_μ and ϕ_μ are the spacelike unity vectors along, respectively, $r-$, $\theta-$, and $\phi-$directions, and ρ, p_r and $p_\perp$ are the energy density and pressures along the radial and tangential directions. To the leading order, they are given by:

$$\rho \simeq \frac{4\alpha_1^2m^2 - d_1}{d_1 r^2}, \quad p_r \simeq -\frac{d_1 + 4\alpha_1^2m^2}{d_1 r^2}, \quad p_\perp \simeq \frac{4\alpha_1^2m^2}{d_1 r^2}, \tag{79}$$

which all approach zero as r^{-2}. This is also consistent with the asymptotical behaviors of the quantities given in Equation (72).

It should be also noted that, despite these differences, the spacetimes of the current solutions are also asymptotically flat and the corresponding ADM masses are as well defined as that of the AOS solution [55].

3.3. External Spacetimes with $\alpha_1 = 0$

When $\alpha_1 = 0$, from Equation (62) and Figure 2 we find that this can be the case only when

$$\Omega_b \equiv \omega_{bb} + \omega_{bc} = 0. \tag{80}$$

It is clear that the BMM choices of f_i and δ_i, given by Equations (13) and (26), are not compatible with this case, too.

Then, to the leading order, Equation (61) yields:

$$t_b \simeq t_c \equiv t, \tag{81}$$

as $t_c \to \infty$. With Equations (80) and (81) we find that:

$$\begin{aligned} g_{xx} &\simeq e^{-2t}\left(c_1 e^{2b_o t} + c_2 e^{b_o t} + c_3 + \cdots\right) \\ g_{\theta\theta} &\simeq 4m^2 e^{2t}, \end{aligned} \tag{82}$$

where c_n's are still given by Equation (67). Finding the asymptotic limit of g_{tt} is not so straightforward, and this is mainly because of the term C_{bc} seen in the expression:

$$g_{tt} = \frac{\gamma^2 |p_c| \delta_b^2}{\sinh^2(\delta_b b) C_{bc}^2}. \tag{83}$$

The numerator of C_{bc} in Equation (59) is equal to 1 with the choice of $\omega_{bb} + \omega_{bc} = 0$ and the remainder of g_{tt} is evaluated with the help of Mathematica, and is given by:

$$g_{tt} = e^{2t}\left(d_1 e^{2b_o t} + d_2 e^{b_o t} + d_3 + \cdots\right), \tag{84}$$

where d_ns are also given by Equation (67). Introducing the new coordinates,

$$r = 2me^t, \quad x = \frac{4b_o^2}{(b_o+1)^2}\tau, \tag{85}$$

we find

$$ds^2 = -g_{\tau\tau} d\tau^2 + g_{rr} dr^2 + r^2 d\Omega^2, \tag{86}$$

where

$$\begin{aligned} g_{\tau\tau} &\simeq \left(\frac{r}{2m}\right)^{2(b_o-1)}\left(1 + \frac{c_2}{c_1}\left(\frac{2m}{r}\right)^{b_o} + \frac{c_3}{c_1}\left(\frac{2m}{r}\right)^{2b_o}\right), \\ g_{rr} &\simeq \frac{d_1}{4m^2}\left(\frac{r}{2m}\right)^{2b_o} + \frac{d_2}{4m^2}\left(\frac{r}{2m}\right)^{b_o} + \frac{d_3}{4m^2}. \end{aligned} \tag{87}$$

Then, we find:

$$\begin{aligned}
g^{\mu\nu}R_{\mu\nu} &\simeq \left(\frac{2m}{r}\right)^2\left[\frac{1}{2m^2}+\frac{2(2b_o-1)}{d_1\xi^2}+\mathcal{O}\left(\frac{1}{\xi^3}\right)\right],\\
R^{\mu\nu}R_{\mu\nu} &\simeq \left(\frac{2m}{r}\right)^4\left[\frac{1}{8m^4}-\frac{b_o(c_1d_2-c_2d_1)}{2c_1d_1^2m^2\xi^3}+\mathcal{O}\left(\frac{1}{\xi^4}\right)\right],\\
R^{\mu\nu\alpha\beta}R_{\mu\nu\alpha\beta} &\simeq \left(\frac{2m}{r}\right)^4\left[\frac{1}{4m^4}-\frac{2}{d_1m^2\xi^2}+\mathcal{O}\left(\frac{1}{\xi^3}\right)\right],\\
C^{\mu\nu\alpha\beta}C_{\mu\nu\alpha\beta} &\simeq \left(\frac{2m}{r}\right)^4\left[\frac{1}{12m^4}+\frac{4(b_o-2)}{3d_1m^2\xi^2}+\mathcal{O}\left(\frac{1}{\xi^3}\right)\right];
\end{aligned} \tag{88}$$

here, $\xi \equiv (r/2m)^{b_o}$. Interestingly, the spacetime is again asymptotically flat, and to the leading order has the same asymptotic behavior as that in the case $\alpha_1 \neq 0$. In particular, all these scalars are asymptotically independent of the mass parameter m, and approach zero as r^{-4}, sharply in contrast to the relativistic case given by Equation (75). However, different from the case $\alpha_1 \neq 0$, to the next leader order the Kretschmann scalar behaves like $\mathcal{O}\left(1/r^{2(2+b_o)}\right)$.

To study this case in more details, let us first note that to the leading order the metric takes the form:

$$\begin{aligned}
ds^2 \simeq\ & -c_1\left(\frac{r}{2m}\right)^{2(b_o-1)}dT^2+\frac{d_1}{4m^2}\left(\frac{r}{2m}\right)^{2b_o}dr^2\\
&+r^2d\Omega^2,
\end{aligned} \tag{89}$$

for $r \gg 2m$. Clearly, this is still different from Equation (77) for the AOS solution, despite the fact that, to the leading order, the Kretschmann scalar approaches zero like r^{-4} in both cases. However, because the $r-$dependence of the g_{rr} component, to the next leading order, the Kretschmann scalar approaches zero like $\mathcal{O}\left(1/r^{2(2+b_o)}\right)$. Recall that $b_o \equiv \sqrt{1+\gamma^2\delta_b^2} \geq 1$. This can be further understood by the analysis of the corresponding effective energy-momentum tensor, which can be also cast in the form of Equation (78), but now with,

$$\begin{aligned}
&\rho = -\frac{1}{r^2}\left(1+\frac{4m^2(2b_o-1)}{d_1\left(\frac{r}{2m}\right)^{2b_o}}\right), \quad p_r = \frac{1}{r^2}\left(-1+\frac{4m^2(2b_o-1)}{d_1\left(\frac{r}{2m}\right)^{2b_o}}\right),\\
&p_\perp = -\frac{4m^2(2b_o-1)}{d_1r^2\left(\frac{r}{2m}\right)^{2b_o}},
\end{aligned} \tag{90}$$

which are consistent with the behaviors of the quantities given in Equation (88). Following [55], it is not difficult to see that the spacetimes of the current solutions are also asymptotically flat and the corresponding ADM masses are as well defined as that of the AOS solution.

4. Canonical Phase Space Approach: Internal Spacetimes

In the internal region of the LQBH, the dynamical Equations (43) and (44) take the form

$$\frac{db}{dt_b} = -\frac{1}{2}\left(\frac{\sin(\delta_b b)}{\delta_b}+\frac{\gamma^2\delta_b}{\sin(\delta_b b)}\right), \tag{91}$$

$$\frac{dp_b}{dt_b} = \frac{1}{2}p_b\cos(\delta_b b)\left(1-\frac{\gamma^2\delta_b^2}{\sin^2(\delta_b b)}\right), \tag{92}$$

for the variables (b, p_b), and

$$\frac{dc}{dt_c} = -2\frac{\sin(\delta_c c)}{\delta_c}, \tag{93}$$

$$\frac{dp_c}{dt_c} = 2p_c\cos(\delta_c c), \tag{94}$$

for (c, p_c). Equations (91) and (92) are identical to Equations (17) and (18), if we replace T by t_b, while Equations (93) and (94) are identical with Equations (19) and (20), if we replace T by t_c. Then, the corresponding solutions can be obtained directly from Equations (21)–(24) by the above replacements, which lead to:

$$\cos(\delta_b b) = b_o\frac{1+b_o\tanh\left(\frac{b_o t_b}{2}\right)}{b_o+\tanh\left(\frac{b_o t_b}{2}\right)} = b_o\frac{b_+e^{b_o t_b}-b_-}{b_+e^{b_o t_b}+b_-},$$

$$p_b = -\frac{mL_o}{2b_o^2}\left(b_+ + b_-e^{-b_o t_b}\right)\mathfrak{A}, \tag{95}$$

$$\sin(\delta_c c) = \frac{2a_o e^{2t_c}}{a_o^2+e^{4t_c}},$$

$$p_c = 4m^2\left(a_o^2+e^{4t_c}\right)e^{-2t_c}, \tag{96}$$

but now with

$$\mathfrak{A} \equiv \left[2\left(b_o^2+1\right)e^{b_o t_b}-b_-^2-b_+^2e^{2b_o t_b}\right]^{1/2}, \tag{97}$$

where a_o and $b_\pm$ are still given by Equation (23), and the range of the variables is given by Equation (24). Then, it can be seen that the two Dirac observables O_b and O_c are also given by Equation (25) along the dynamical trajectories. However, instead of imposing the conditions (26), now we shall leave the choice of δ_b and δ_c open, as we did in the last section. Thus, the corresponding internal spacetimes are described by the metric:

$$ds^2 = -N^2dT^2+\frac{p_b^2}{|p_c|L_o^2}dx^2+|p_c|d\Omega^2$$

$$= -\left(\frac{N}{C_{cb}}\right)^2dt_c^2+\frac{p_b^2}{|p_c|L_o^2}dx^2+|p_c|d\Omega^2, \tag{98}$$

where

$$N \equiv \frac{\gamma\delta_b\,\mathrm{sgn}(p_c)|p_c|^{1/2}}{\sin(\delta_b b)} = \frac{2m}{\mathfrak{A}}\left(b_+e^{b_o t_b}+b_-\right)\left(a_o^2e^{-2t_c}+e^{2t_c}\right)^{1/2}. \tag{99}$$

In the following, let us study the above spacetimes near the horizons ($\mathfrak{A}=0$) and throat ($\partial p_c/\partial t_c = 0$), separately.

4.1. Spacetimes near the Horizons

The horizons now are located at $\mathfrak{A}=0$, which yields two solutions:

$$t_b^{\mathrm{BH}} = 0, \quad t_b^{\mathrm{WH}} = -\frac{2}{b_o}\ln\left(\frac{b_o+1}{b_0-1}\right). \tag{100}$$

Now to find the relation between t_b and t_c the following expression has to be integrated:

$$dt_c = \frac{C_{cb}}{C_{bc}}dt_b, \tag{101}$$

where the expressions of C_{bc} and C_{cb} in the interior are:

$$\begin{aligned} C_{bc} &= \frac{1}{\mathcal{D}}\left(1-\Omega_c\frac{\partial O_c}{\partial \delta_c}\right), \\ C_{cb} &= \frac{1}{\mathcal{D}}\left(1-\Omega_b\frac{\partial O_b}{\partial \delta_b}\right), \end{aligned} \tag{102}$$

but now with

$$\begin{aligned} \mathcal{D} &\equiv 1-\omega_{cc}\frac{\partial O_c}{\partial \delta_c}-\omega_{bb}\frac{\partial O_b}{\partial \delta_b}+(\omega_{bb}\omega_{cc}-\omega_{bc}\omega_{cb})\frac{\partial O_b}{\partial \delta_b}\frac{\partial O_c}{\partial \delta_c}, \\ \frac{\partial O_b}{\partial \delta_b} &= -\frac{p_b}{2\gamma L_o\delta_b^2}\left(1-\frac{\gamma^2\delta_b^2}{\sin^2(\delta_b b)}\right)\left[\delta_b b\cos(\delta_b b)-\sin(\delta_b b)\right], \\ \frac{\partial O_c}{\partial \delta_c} &= \frac{p_c}{\gamma L_o\delta_c^2}\left[\delta_c c\cos(\delta_c c)-\sin(\delta_c c)\right]. \end{aligned} \tag{103}$$

Similar to the previous subsection, in the following section we consider the cases $\alpha_1 = 0$ and $\alpha_1 \neq 0$, separately.

4.1.1. $\alpha_1 = 0$

In this case, it is remarkable to note that by integrating Equation (56) we find the following explicit solution,

$$t_b = t_b^0 + t_c + \frac{m\Omega_c}{\delta_c}\left\{\cosh(2\mathcal{T})\tan^{-1}\left(e^{2\mathcal{T}}\right)-\cosh[2(t_c-\mathcal{T})]\tan^{-1}\left[e^{-2(t_c-\mathcal{T})}\right]\right\}, \tag{104}$$

which holds for any t_c, including the region $t_c \geq 0$, outside the black hole horizon, where $t_c = \mathcal{T}$ is the location of the transition surface, defined by Equation (27). Additionally, t_b^0 is an integration constant which will be set to zero in the following discussions. When $t_c = 0$ the second term in the right-hand side of the above expression vanishes identically, and as $t_c \to \infty$ it goes to zero as $\mathcal{O}\left(e^{-2t_c}\right)$. This is consistent with Equation (61).

In Figure 3, we plot the curves of t_b vs t_c of Equation (104) for different choices of parameters involved. In particular, we find that the properties of t_b across the transition surface sensitively depend on the signs of Ω_c. More specifically, when $\Omega_c > 0$, t_b decreases exponentially right after crossing the transition surface, as t_c becomes more and more negative, as shown by Curves b, c and d with the choice $\Omega_c = 0.5$, where the dots on the curves mark the locations of the transition surfaces. On the other hand, when $\Omega_c < 0$, t_b increases exponentially right after crossing the transition surface, as shown by Curves b', c' and d' with $\Omega_c = -0.5$. However, the locations of the transition surface indeed depend on the choices of the parameters $(m,\ L_0\delta_c)$, as shown by Equation (27). In particular, Curves b, c and d respectively correspond to:

$$\left(\frac{m}{m_p}, \frac{L_o\delta_c}{\ell_p}\right) = \left\{\left(10^6, 10^{-7}\right), \left(10^6, 0.1\right), (1, 0.1)\right\},$$

while Curves b', c' and d' are all for the same choices of (m, δ_c), as that of the unprimed curves in respective order. Curves b and c share the same mass, i.e., $m/m_p = 10^6$, but with different δ_c's. Meanwhile, the locations of the throats (the gray dots) move from the left-hand side to the right-hand side in the direction closer to the horizon, which means that the quantum effects increase as δ_c increases. Curves c and d share the same $\delta_c = 0.1$, but different masses. Comparing their throat positions, we find that the smaller mass also means the more significant quantum effects. On the other hand, outside the horizon, no matter what the parameters are, $t_b \simeq t_c$, which is consistent with our previous conclusion

for large t_b and t_c, as shown by Equation (81). To understand this point further, let us expand the above expression around the horizon, for which we find:

$$t_b = \beta_1 t_c + \beta_2 t_c^2 + \beta_3 t_c^3 + \mathcal{O}\left(t_c^4\right), \tag{105}$$

where

$$\begin{aligned}
\beta_1 &\equiv 1 + \frac{m\Omega_c}{a_o\delta_c}\left[a_o + \left(a_o^2 - 1\right)\tan^{-1}(a_o)\right],\\
\beta_2 &\equiv -\frac{m\Omega_c}{a_o(a_o^2+1)\delta_c}\left[a_o\left(a_o^2-1\right) + \left(a_o^2+1\right)^2\tan^{-1}(a_o)\right],\\
\beta_3 &\equiv \frac{2m\Omega_c}{3a_o(a_o^2+1)^2\delta_c}\left[a_o + 6a_o^3 + a_o^5 + \left(a_o^2-1\right)\left(a_o^2+1\right)^2\tan^{-1}(a_o)\right].
\end{aligned} \tag{106}$$

For macroscopic black holes, we have $m/m_p \gtrsim M_\odot \simeq 10^{38}$, while the semi-classical limit requires $L_0\delta_c \ll 1$. Then, expanding β_n in terms: of a_o, we find that

$$\begin{aligned}
\beta_1 &= 1 + \frac{m\Omega_c}{a_o\delta_c}\left[a_o + \left(a_o^2-1\right)\tan^{-1}(a_o)\right] \simeq 1 + \frac{\gamma^2 L_o^2\delta_c\Omega_c}{48m} + \mathcal{O}\left(a_o^4\right) \simeq 1,\\
\beta_2 &= -\frac{\gamma^2 L_o^2\delta_c\Omega_c}{24m} + \mathcal{O}\left(a_o^4\right) \simeq 0,\\
\beta_3 &= \frac{\gamma^2 L_o^2\delta_c\Omega_c}{18m} + \mathcal{O}\left(a_o^4\right) \simeq 0.
\end{aligned} \tag{107}$$

Therefore, for macroscopic black holes, the relation $t_b \simeq t_c$ near the horizon is well justified. Then, we find that the metric components take the form:

$$\begin{aligned}
g_{xx} &= \frac{e^{2t_c}\zeta(t_c)^2}{16b_o^4(a_o^2+e^{4t_c})}\left((b_o-1)e^{-b_o t_c} + b_o + 1\right)^2,\\
g_{t_c t_c} &= 4m^2 e^{-2t_c}\left(a_o^2 + e^{4t_c}\right)\frac{\beta_-(t_c)^2}{\zeta(t_c)^2}\left\{1 - \omega_{cc}\frac{\partial O_c}{\partial\delta_c}\right.\\
&\quad + m\omega_{bb}e^{-b_o t_c}\left(\Omega_c\frac{\partial O_c}{\partial\delta_c} - 1\right)\frac{\left(2b_o^2 e^{b_o t_c} - \zeta(t_c)^2\right)}{2\gamma\delta_b^2 b_o^2\zeta(t_c)}\\
&\quad \left.\times\left[\gamma\delta_b\zeta(t_c) - b_o\beta_-(t_c)\cos^{-1}\left(\frac{b_o\beta_-(t_c)}{\beta_+(t_c)}\right)\right]\right\}^2,
\end{aligned} \tag{108}$$

$$\begin{aligned}
\zeta(t_c) &\equiv \left[2\left(b_o^2+1\right)e^{b_o t_c} - (b_o-1)^2 - (b_o+1)^2 e^{2b_o t_c}\right]^{1/2},\\
\beta_\pm(t_c) &\equiv (b_o+1)e^{b_o t_c} \pm (b_o-1).
\end{aligned} \tag{109}$$

To quantify the quantum effects near the horizon, let us compute the Hawking temperature at the horizon. Given a metric of the form:

$$ds^2 = -g_{tt}dt^2 + g_{xx}dx^2 + p_c d\Omega^2, \tag{110}$$

the Hawking temperature of the black hole is given by [55]:

$$T_H = \frac{\hbar}{k_B\mathcal{P}}, \quad \mathcal{P} = \lim_{t\to 0}\frac{4\pi(g_{tt}g_{xx})^{\frac{1}{2}}}{\partial_t g_{xx}}, \tag{111}$$

where k_B is the Boltzmann constant. Then, for the metric coefficients given by Equation (108) we find:

$$T_H = \frac{T_H^{\rm GR}}{(1+a_o^2)(1+\varepsilon_T)}, \tag{112}$$

where $T_H^{\rm GR} = \hbar/(8k_B\pi m)$ denotes the Hawking temperature of the Schwarzschild black hole calculated in GR, and

$$\varepsilon_T \equiv \frac{m\omega_{cc}}{a_o\delta_c}\left[a_o + \left(a_o^2-1\right)\tan^{-1}(a_o)\right]. \tag{113}$$

For a BH of mass 10^6, we find that:

$$a_o^2 = \left(\frac{\gamma\delta_c L_o}{8m}\right)^2 \simeq 10^{-22},$$

and

$$\varepsilon_T = \left(\frac{4m\omega_{cc}}{3\delta_c}\right)\left(1-\frac{2}{5}a_o^2\right)a_o^2 + \mathcal{O}\left(a_o^6\right).$$

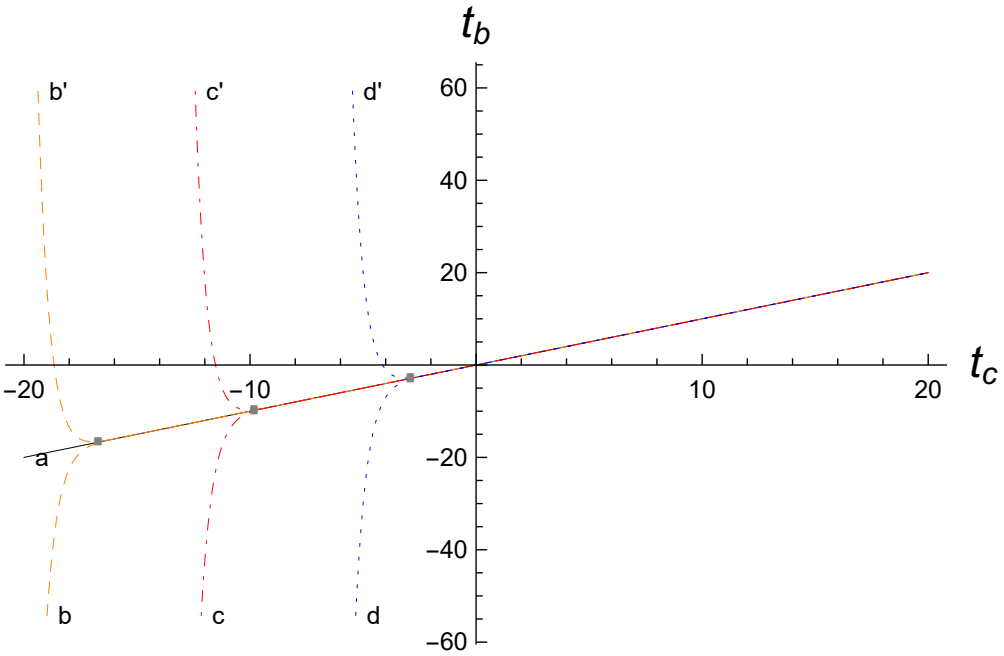

Figure 3. Plots of t_b vs t_c for $\alpha_1 = 0$ defined by Equation (104). Depending on the signs of Ω_c, the dependence of t_b on t_c is different. Curves b, c and d are all for $\Omega_c = 0.5$ but with different choices of (m, δ_c). In particular, they correspond to $(m,\delta_c) = \{(10^6, 10^{-7}), (10^6, 0.1), (1, 0.1)\}$, respectively. Curves b', c' and d' are all for $\Omega_c = -0.5$ but with the same choice of (m, δ_c) as that of the unprimed curves in the respective order.

For the AOS choice of Equation (13), we find that $4m\omega_{cc}/(3\delta_c) \simeq \mathcal{O}(1)$, so that $\varepsilon_T \lesssim 10^{-44}$, that is, for macroscopic black holes, the quantum effects are negligible. This is consistent with what was concluded by AOS [54,55].

The above conclusion can be further verified by comparing the Kretschmann scalars K with its relativistic counterpart $K_{\rm GR} \equiv 48m^2/p_c^3$. In particular, in Figure 4 we plot the relative difference of K and $K_{\rm GR}$ for $m = 10^6 m_{pl}$ and $m = 10^{12} m_{pl}$, which indicate negligible quantum corrections near the horizon for massive LQBHs.

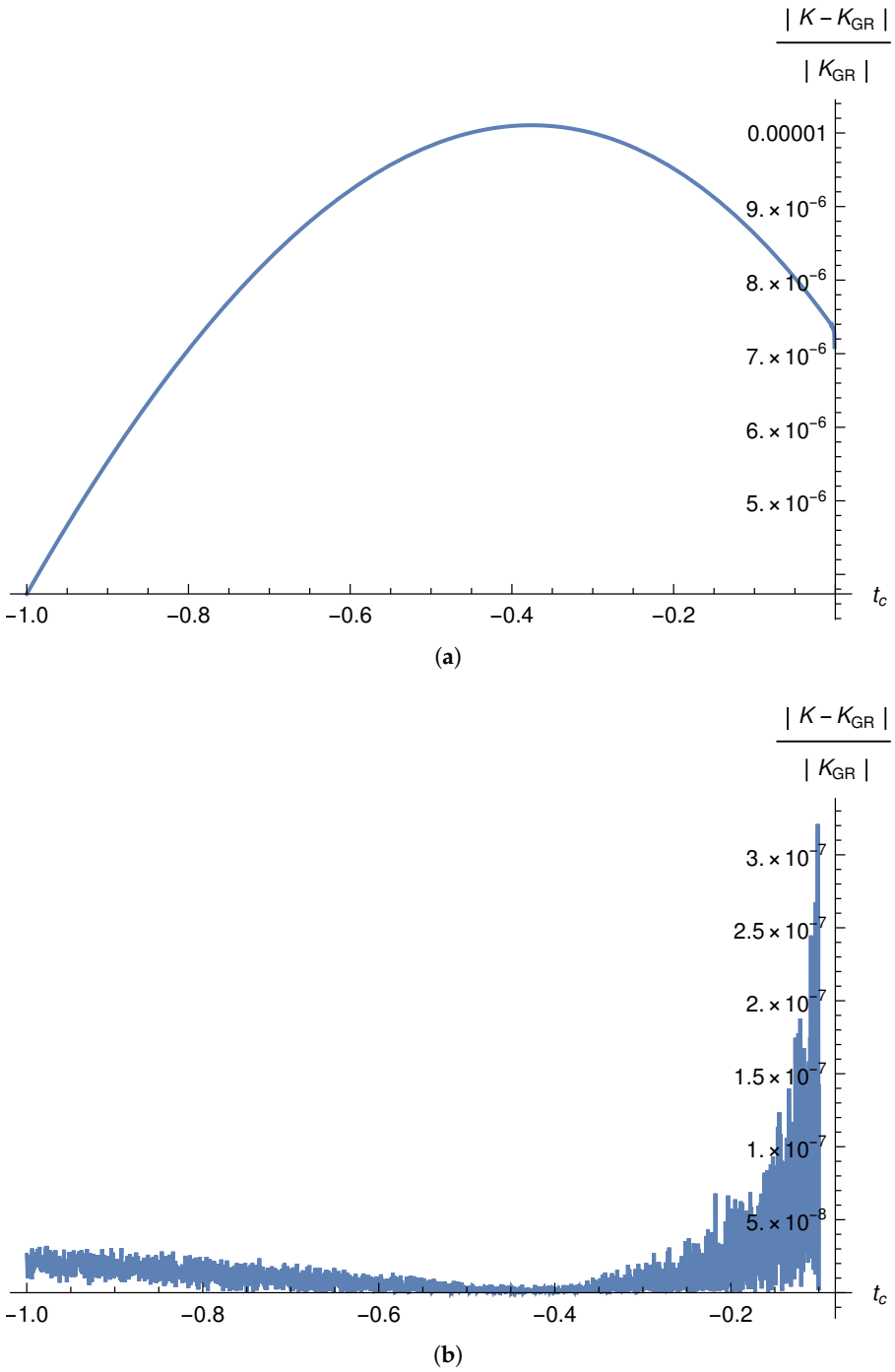

Figure 4. Plots of the relative difference between the Kretschmann scalars K and $K_{\rm GR}$ in the $\alpha_1 = 0$ case, for (**a**) $m = 10^6$, and (**b**) $m = 10^{12}$. Here $K_{\rm GR}(\equiv 48\ {\rm m}^2/{\rm p}_{\rm c}^3)$ is the corresponding Kretschmann scalar given by GR.

4.1.2. $\alpha_1 \neq 0$

When $\alpha_1 \neq 0$, we find that:

$$\begin{aligned} & t_b\left(1+\frac{m\Omega_b}{\delta_b b_o^2}\right)+\frac{2m\Omega_b}{\delta_b b_o^2}-\frac{m\Omega_b}{2\gamma\delta_b^2 b_o^2}e^{-b_o t_b}\beta_+(t_b)\zeta(t_b)\cos^{-1}\left(\frac{b_o\beta_-(t_b)}{\beta_+(t_b)}\right) \\ + & \frac{m\Omega_b}{2\delta_b b_o^3}\left((b_o-1)^2 e^{-b_o t_b}-(b_o+1)^2 e^{b_o t_b}-2b_o^3 t_b\right)+t_b^0 \\ = & t_c+\frac{m\Omega_c}{\delta_c}\left(\cosh(2\mathcal{T})\tan^{-1}\left(e^{2\mathcal{T}}\right)-\cosh(2(t_c-\mathcal{T}))\tan^{-1}\left(e^{-2(t_c-\mathcal{T})}\right)\right), \end{aligned} \quad (114)$$

where t_b^0 is an integration constant and will be set to zero as done previously in the $\alpha_1 = 0$ case.

Notice that the t_c part of the above expression is precisely the right-hand side of Equation (104), and we showed explicitly in the last subsection that near the horizon $t_c = 0$ the right-hand side can be well approximated by t_c. Now, expanding the t_b part of the above expression around the horizon, we find:

$$t_b + \nu_2 t_b^2 + \nu_3 t_b^3 + \mathcal{O}\left(t_b^4\right), \tag{115}$$

where

$$\nu_2 = \frac{1}{6} m\gamma^2 \delta_b \Omega_b, \quad \nu_3 = \frac{1}{60} m\gamma^2 \delta_b \Omega_b \left(10 - \gamma^2 \delta_b^2\right). \tag{116}$$

The above coefficients ν_i are negligibly small for large black holes. For example, for a BH of mass 10^6, they are of the order $\sim 10^{-9}$. Hence, for macroscopic black holes Equation (114) can also be well approximated by:

$$t_b \simeq t_c, \tag{117}$$

near the black hole horizon, similar to the case $\alpha_1 = 0$. This linear relation can be confirmed by the plot of Equation (114) for various values, as seen in Figure 5. For plotting the curves b, c, and d corresponding to positive Ω_c, the parameters are chosen respectively as:

$$\begin{aligned} &\left(\frac{m}{m_p}\right) = \left(10^6, 10^8, 10^{10}\right), \quad (\omega_{cc}, \omega_{cb}, \Omega_c) = \left(\frac{\delta_c}{3m}, 0, \frac{\delta_c}{3m}\right), \\ &(\omega_{bb}, \omega_{bc}, \Omega_b) = \left(\frac{\delta_b}{3m}, 0, \frac{\delta_b}{3m}\right), \end{aligned} \tag{118}$$

where δ_i's are given by Equation (26).

Since in the current case, ($\alpha_1 \neq 0$) $t_b \simeq t_c$ also holds near the horizon for macroscopic black holes, the thermodynamics of the black hole horizon is quite similar to the case $\alpha_1 = 0$. In particular, its temperature is also given by Equations (112) and (113), and the difference to that of the Schwarzschild black hole calculated in GR is negligibly small for macroscopic black holes.

Again, a plot of the relative difference between the Kretschmann scalar K and K_{GR} is given in Figure 6 for the $\alpha_1 \neq 0$ case, which also shows the negligible quantum effects near the horizons for massive LQBHs.

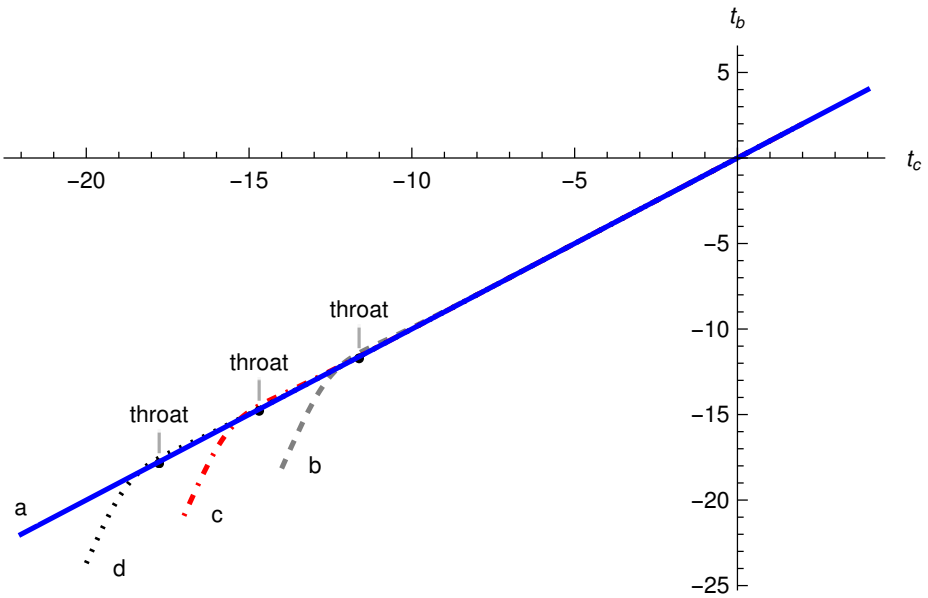

Figure 5. Plots of Equation (114) for various choices as given by Equation (118).

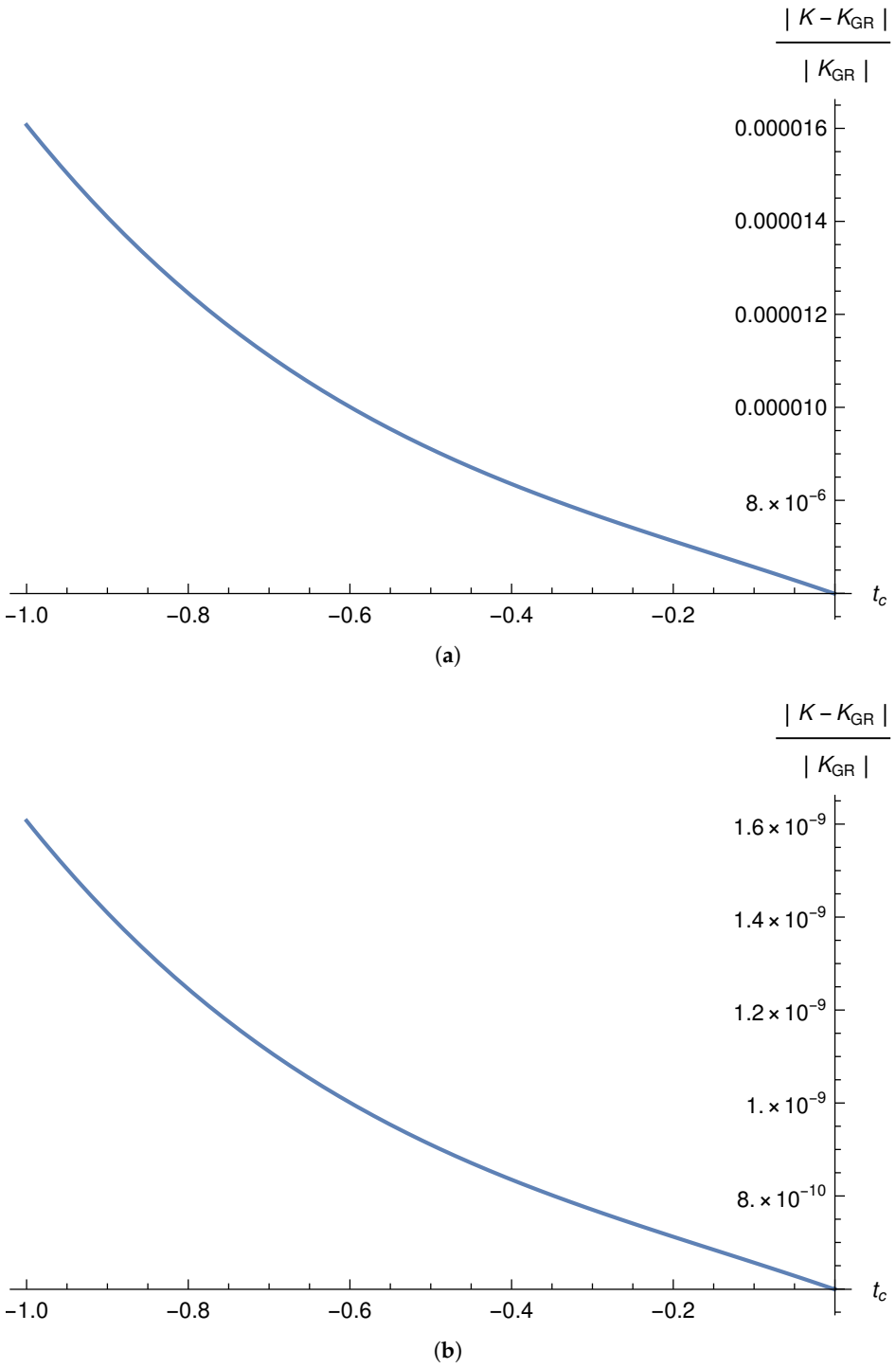

Figure 6. Plots of the relative difference between the Kretschmann scalars K and $K_{\rm GR}$ in the $\alpha_1 \neq 0$ case, for (**a**) $m = 10^6$, and (**b**) $m = 10^{12}$.

4.2. Spacetimes near Transition Surfaces

It is evident from Figures 3 and 5 that the above approximation, $t_b \simeq t_c$, is no longer valid once we start to probe the spacetime near and to the other side of the transition surface. We break this analysis again into two cases, $\alpha_1 = 0$ and $\alpha_1 \neq 0$.

4.2.1. $\alpha_1 = 0$

In this case, the relation between t_b and t_c is given by Equation (104), which is valid everywhere in the interior. Combining this equation with the metric (98), we can calculate

the curvature invariants to analyze the spacetime near the transition surface. We find that this can be performed by xAct [63], a package for tensor computations in Mathematica, although the exact expressions are too complicated to be written down here. For this reason, we only plot out the Kretschmann scalar here for illustration, as other scalars such as the Ricci scalar, Ricci tensor squared, have similar features. In particular, in Figures 7 and 8 we plot the Kretschmann scalar, respectively, for $\Omega_c < 0$ and $\Omega_c > 0$, but all with $\Omega_b = 0$. In addition, we also provide Table 1, in which we show the explicit dependence of the maximal amplitude K_m of the Kretschmann scalar on the mass m, the location of the maximal amplitude of the Kretschmann scalar, denoted by τ_m, and the location of the transition surface denoted by $\tau_{\rm ts}$. To compare with the AOS solution, we also provide the maximal amplitudes of the Kretschmann scalar for the AOS solution.

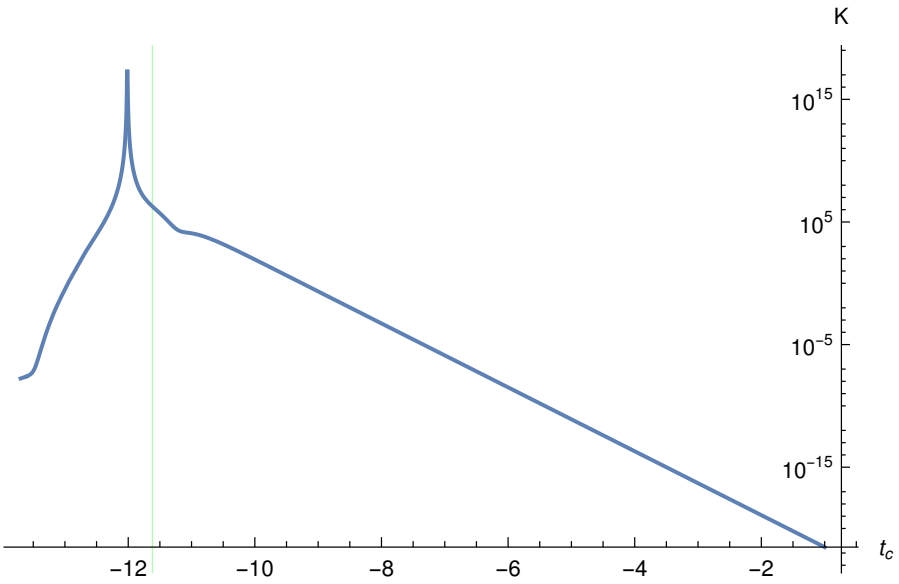

Figure 7. The Kretschmann scalar near the transition surface $\tau_{ts} \simeq -11.6201$ denoted by the vertical line for the case $\alpha_1 = 0$. Here $m = 10^6$, $(\omega_{cc}, \omega_{cb}) = (-\delta_c/3m, 0)$, and $(\omega_{bb}, \omega_{bc}) = (-\delta_b/3m, \delta_b/3m)$, so that $(\Omega_b, \Omega_c) = (0, -\delta_c/3m < 0)$, where δ_i's are given by Equation (26).

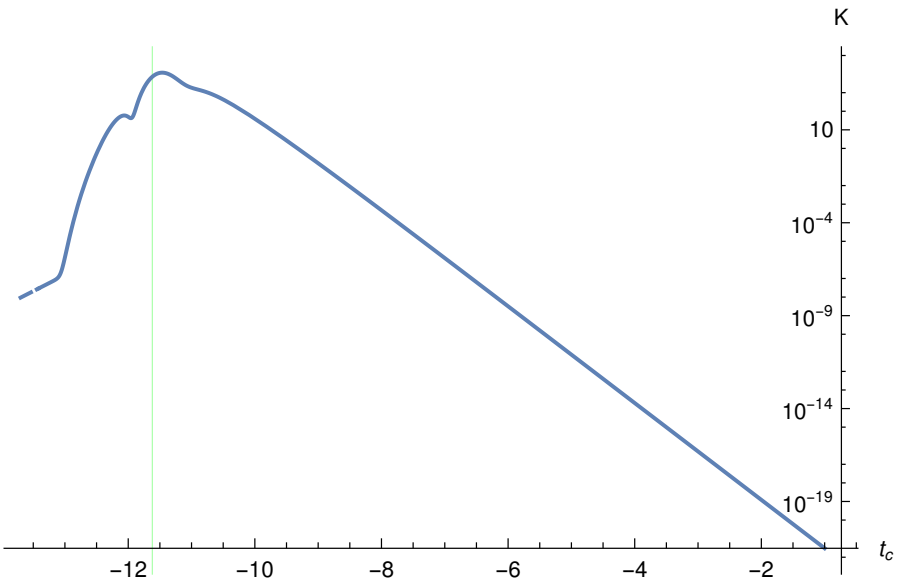

Figure 8. The Kretschmann scalar near the transition surface denoted by the vertical line for the case $\alpha_1 = 0$. Here $m = 10^6$, $(\omega_{cc}, \omega_{cb}) = (\delta_c/3m, 0)$, and $(\omega_{bb}, \omega_{bc}) = (\delta_b/3m, -\delta_b/3m)$, so that $(\Omega_b, \Omega_c) = (0, \delta_c/3m > 0)$, where δ_i's are given by Equation (26).

From Figures 7 and 8 and Table 1 we can see that the Kretschmann scalar remains finite across the transition surfaces, but the maximal amplitude of the Kretschmann scalar sensitively depends on the mass m, which is in sharp contrast to the AOS solution in which the maximal amplitude K_m^{AOS} of the Kretschmann scalar remains the same [53–55].

Table 1. The maximal amplitude K_m of the Kretschmann scalar K for the case $\alpha_1 = 0$ with different choices of the mass parameter m. Here τ_m denotes the location of the maximal point of K, and τ_{ts} the location of the corresponding transition surface (throat). To compare it with that given by the AOS solution, we also give the maximal values of K_m^{AOS}. Here we choose $\omega_{bb} = -\delta_b/3m$, $\omega_{bc} = \delta_b/3m$, $\omega_{cc} = -\delta_c/3m$, and $\omega_{cb} = 0$, so that $(\Omega_b, \Omega_c) = (0, -\delta_c/3m < 0)$, where δ_i's are given by Equation (26).

m/m_p	τ_m	K_m	τ_{ts}	K_m^{AOS}
10^6	-12.0147	2.46×10^{48}	-11.6201	82,188.3628
10^8	-15.0848	1.56×10^{52}	-14.6902	82,188.3642
10^{10}	-18.1549	3.60×10^{75}	-17.7603	82,188.3642
10^{12}	-21.225	2.21×10^{75}	-20.8304	82,188.3642
10^{14}	-24.2951	2.87×10^{70}	-23.9005	82,188.3642
10^{16}	-27.3653	2.82×10^{69}	-26.9706	82,188.3641
10^{18}	-30.4354	9.59×10^{77}	-30.0408	82,188.3618

Another unexpected feature is that *the maximal point of the Kretschmann scalar usually is not precisely at the transition surface*, $\tau_m \neq \tau_{ts}$. Although this looks strange, a closer examination shows that this is due to two main facts: (1) the appearance of the factor $1/C_{bc}$ in the lapse function of the metric (98), and (2) the dependence of t_b on t_c, which will lead to the modifications of $g_{xx}(t_b, t_c)$, in comparison to the corresponding AOS component $g_{xx}^{\rm AOS}(t_b, t_c)$ in which we have $t_b = t_c = T$.

In particular, when $\alpha_1 = 0$, we have $1/C_{bc} = \mathcal{D}$, as can be seen from Equation (102), where $\mathcal{D}$ is defined by Equation (103). In Figure 9 we plot out the function $\mathcal{D}^2$ for the same choices of the parameters as given in Figure 7, from which we can see that it changes dramatically near the maximal point $\tau_m \simeq -12.0147$ of the Kretschmann scalar. In Figures 10 and 11, we plot out the metric components $g_{t_c t_c}$ and g_{xx} given in Equation (98) vs. t_c, where $g_{tt} \equiv |g_{t_c t_c}|$. From these figures we can see clearly that both of these components change dramatically near the maximal point τ_m of the Kretschmann scalar. To compare it with the AOS solution, in each of these two figures, we also plot the corresponding quantities for the AOS solution, from which it can be seen that no such behavior appears in the AOS solution.

We also study the location of the white horizon and find that it is very near the transition surface. In particular, the ratio between WH and BH horizon radii now is much smaller than 1 and sensitively depends on the mass parameter m, as shown explicitly in Table 2. Whereas in the AOS model this ratio is very close to 1.

Table 2. The ratio of the WH and BH horizon radii for the case $\alpha_1 = 0$ with different choices of the mass parameter m. Here we use the same choices as those in Figure 8, except for m.

m/m_p	$\frac{r_{WH}}{r_{BH}}$
10^6	5.5872×10^{-5}
10^8	2.9462×10^{-6}
10^{10}	1.5148×10^{-7}
10^{12}	7.6577×10^{-9}
10^{14}	3.8242×10^{-10}
10^{16}	1.8923×10^{-11}
10^{18}	9.2972×10^{-13}

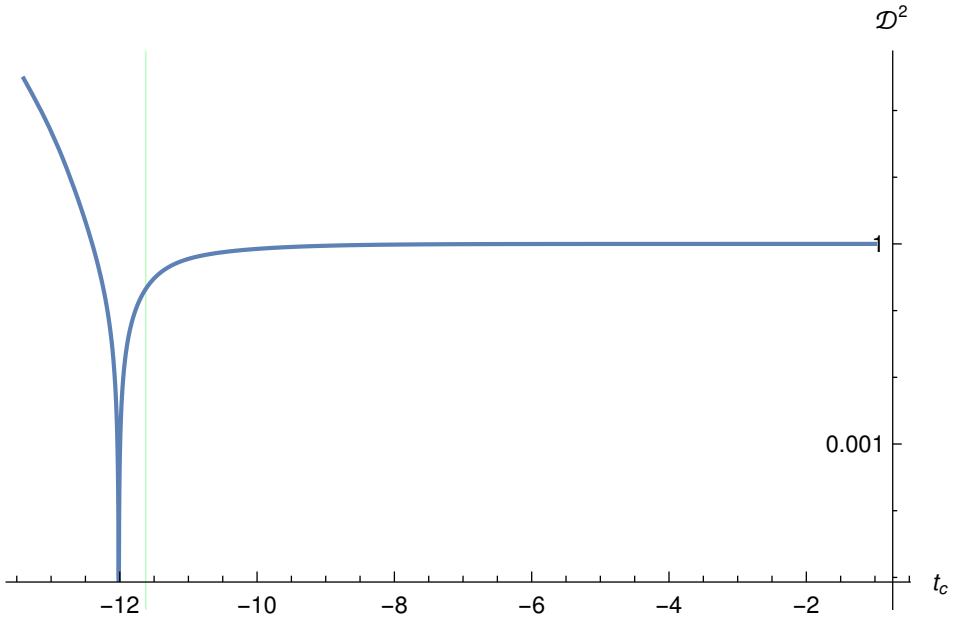

Figure 9. The function $\mathcal{D}^2$ defined by Equation (103) for the case $\alpha_1 = 0$, for which we have $C_{bc} = 1/\mathcal{D}$. The vertical (green) line marks the position of the transition surface. When plotting this curve, we have chosen the relevant parameters exactly as those given in Figure 7.

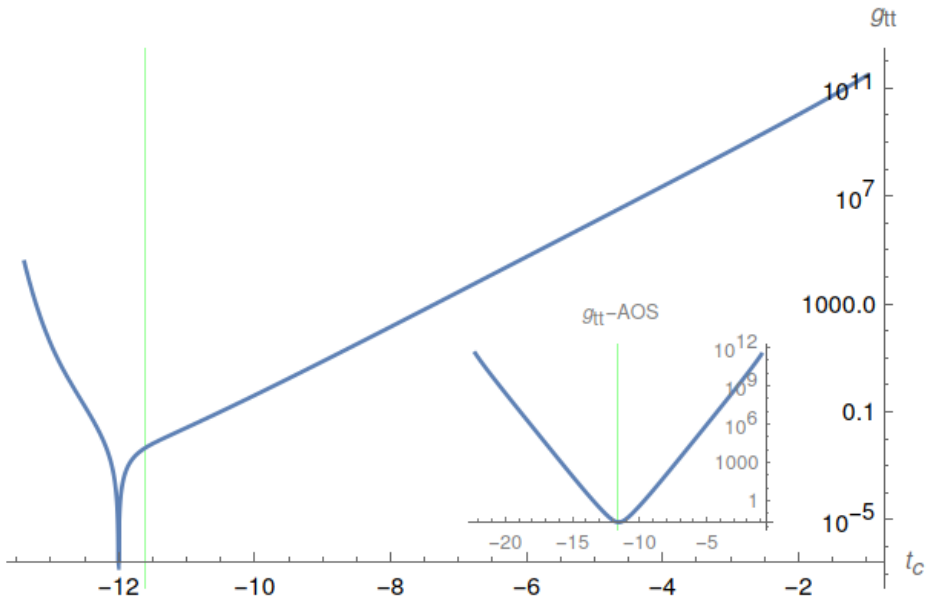

Figure 10. The metric component $g_{t_c t_c}$ given in Equation (98), where $g_{tt} \equiv |g_{t_c t_c}|$. The inserting is the plot of the same quantity for the AOS solution. When plotting this curve, we have chosen the relevant parameters exactly as those given in Figure 7.

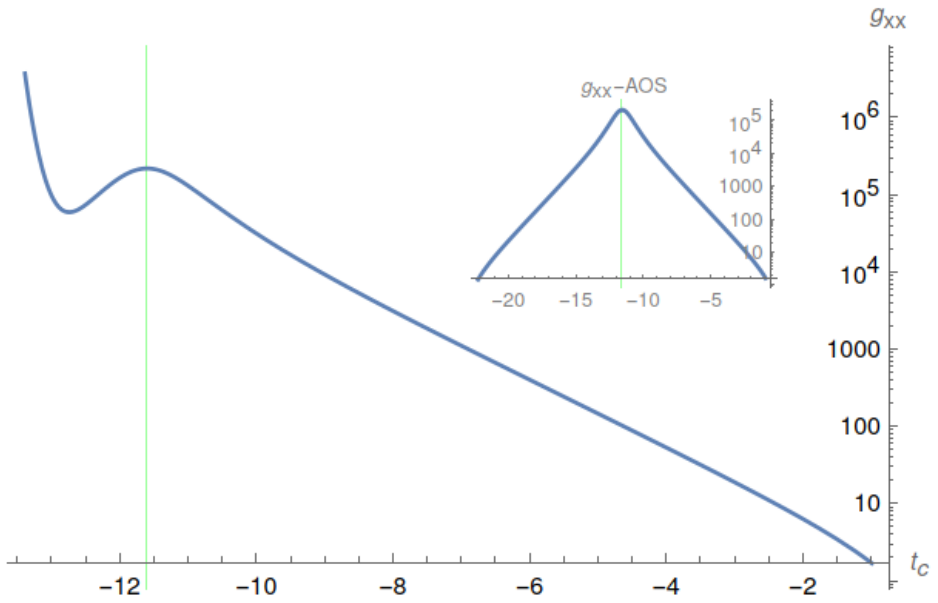

Figure 11. The metric component g_{xx} given in Equation (98). The inserting is the plot of the same quantity for the AOS solution. When plotting this curve, we have chosen the relevant parameters exactly as those given in Figure 7.

4.2.2. $\alpha_1 \neq 0$

In this case, the explicit relation between t_b and t_c is given by Equation (114). This relation allows us to write down the metric and calculate the curvature invariants. Similar to the $\alpha_1 = 0$ case, the exact expressions of them are too complicated to be written down explicitly here, and instead we find that it sufficient to simply plot them out. Since they all have similar behavior, we plot out only the Kretschmann scalar. In particular, we plot it for $\Omega_c < 0$ and $\Omega_c > 0$, respectively in Figures 12 and 13. The vertical line in each of these figures represents the location of the transition surface, and is usually different from the maximal point of the Kretschmann scalar, quite similar to the case $\alpha_1 = 0$ and for similar reasons.

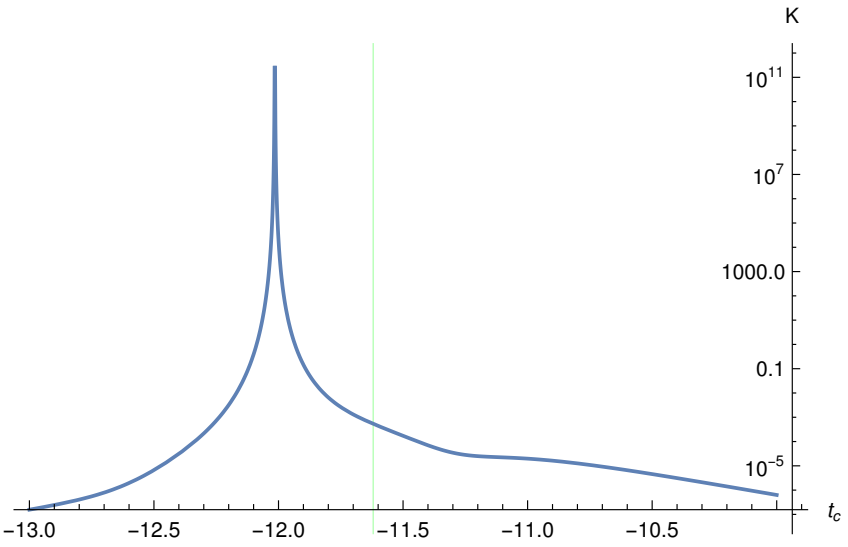

Figure 12. The Kretschmann scalar for the case $\alpha_1 \neq 0$ with $\Omega_c < 0$. In particular, the parameters are chosen as $m = 10^6$, $(\omega_{cc}, \omega_{cb}, \Omega_c) = (-\frac{\delta_c}{3m}, 0, -\frac{\delta_c}{3m})$, $(\omega_{bb}, \omega_{bc}, \Omega_b) = (-\frac{\delta_b}{3m}, 0, -\frac{\delta_b}{3m})$, where δ_i's are given by Equation (26).

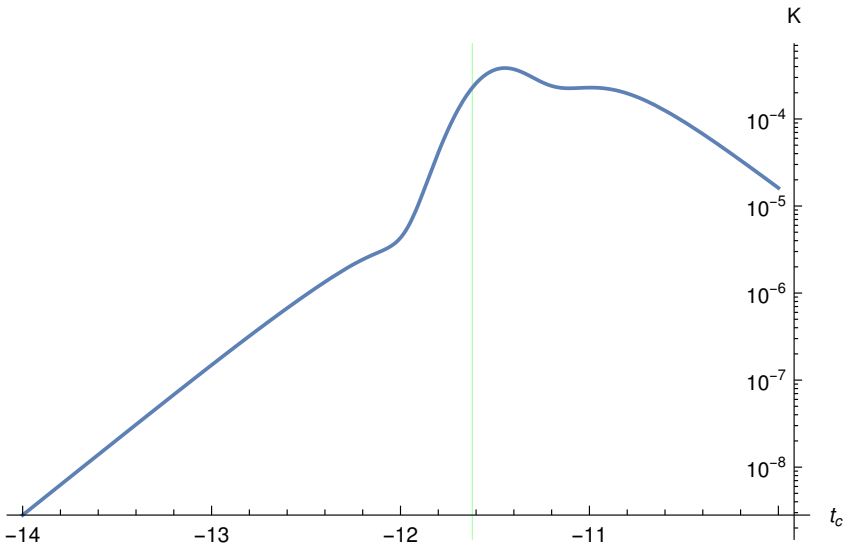

Figure 13. The Kretschmann scalar for the case $\alpha_1 \neq 0$ with $\Omega_c > 0$. In particular, the parameters are chosen as $m = 10^6$, $(\omega_{cc}, \omega_{cb}, \Omega_c) = (\frac{\delta_c}{3m}, \frac{\delta_c}{3m}, \frac{2\delta_c}{3m})$, $(\omega_{bb}, \omega_{bc}, \Omega_b) = (\frac{\delta_b}{3m}, \frac{\delta_b}{3m}, \frac{2\delta_b}{3m})$, where δ_i's are given by Equation (26).

5. Conclusions

In this paper, we studied the 4-dimensional canonical phase space approach, explored respectively by BMM [59] and GM [60] recently, in which the two parameters δ_i $(i = b, c)$ appearing in the polymerization quantization [35],

$$b \to \frac{\sin(\delta_b b)}{\delta_b}, \quad c \to \frac{\sin(\delta_c c)}{\delta_c}, \tag{119}$$

are considered functions of the two Dirac variables O_b and O_c [60],

$$\delta_i = f_i(O_b, O_c), \ (i, = b, c), \tag{120}$$

where O_b and O_c are given by Equations (10) and (11). Note that BMM only considered the particular case $\delta_i = f_i(O_i)$ [59], the same as the AOS choice given in Equation (14), although AOS considered them in the extended 8-dimensional phase space $\Gamma_{\rm ext}$. The corresponding dynamical equations are given by Equations (48) and (49), which allow analytical solutions in terms of t_b and t_c, where t_b and t_c are all functions of T only, given by Equation (47).

To compare the AOS and BMM/GM approaches, in Section 2 we first presented the AOS model, and discuss how to uniquely fix the two Dirac observables δ_i's [cf. Equations (15) and (16)] in the extended phase space. In the large mass limit, these conditions lead to δ_i's given explicitly by Equation (26).

In the BMM/GM model, the black and white horizons, in general, all exist, and naturally divide the whole spacetime into the external and internal regions, where T is timelike in the internal region and spacelike in the external region. In Section 3, we briefly introduce the BMM/GM approach and focused on studies of the external region of the spacetime. We found that the asymptotical flatness condition of the spacetime requires

$$\Omega_b \geq 0, \tag{121}$$

where Ω_b is defined in Equation (60), which excludes the BMM choice $\delta_i = f_i(O_i)$ [59], for which we always have $\Omega_b^{\rm BMM} < 0$, as shown explicitly by Equation (63). Despite the significant difference of the metrics of the AOS and BMM/GM models, we found that, to the leading order, the asymptotical behavior of the spacetime in the two models is universal and independent of the mass parameter m for the curvature invariants [cf.

Equations (72) and (88)]. However, to the next leading order, they are different. In particular, the Kretschmann scalar behaves as:

$$K \simeq \frac{A_0}{r^4} + \mathcal{O}\left(\frac{1}{r^4\xi}\right), \tag{122}$$

as $r \to \infty$, where A_0 is a constant and independent of m, and r the geometric radius of the two-spheres. For the case $\alpha_1 \neq 0$, we have $\xi = \frac{2}{\alpha_0}\ln\left(\frac{r}{2m}\right)$, and for $\alpha_1 = 0$, we have $\xi = \left(\frac{r}{2m}\right)^{b_o}$. Here α_1 is defined in Equation (62). The differences from the next leading order can be understood more clearly from the metric and the effective energy-momentum tensor, given, respectively, by Equations (76), (79), (89) and (90). On the other hand, asymptotically, the AOS solution takes the global monopole form (77), found previously in a completely different content [62]. Nevertheless, the leading behavior of the Kretschmann scalar in both cases is in sharp contrast to the classical case [55,57], for which we have $K_{\rm GR} = 48\ {\rm m}^2/{\rm r}^6$.

In Section 4, we conducted our studies on the internal region of the spacetime. We first showed that the quantum gravitational effects near the black hole horizon are negligible for massive black holes, and both the Kretschmann scalar and Hawking temperature are indistinguishable from those of GR, as shown explicitly by Figures 4 and 6, and Equation (112). However, despite the fact that all the physical quantities are finite, and the Schwarzschild black hole singularity is replaced by a transition surface whose radius is always finite and non-zero, the internal region near the transition surface is dramatically different from that of the AOS model in several respects: (1) First, the location of the maxima of the curvature invariants, such as the Kretschmann scalar is displaced from the transition surface as shown explicitly by Figures 7, 8, 12 and 13. Detailed investigations of the metric components reveal that this is because of the dependence of the two Dirac observables δ_i's on the 4D phase space of the Ashtekar variables (b, c, p_b, p_c), which considerably modifies the structure of the spacetime. In particular, we plotted the metric components $g_{t_c t_c}$ and g_{xx}, respectively in Figures 10 and 11, and then compared them with those given in the AOS model, where the maxima are always located at the transition surface [53–55]; (2) The maxima of these curvature invariants depend on the choice of the mass parameter m. In particular, Table 1 shows such dependence for the Kretschmann scalar, which also shows that such dependence is absent in the AOS model; (3) The location of the white hole horizon is very near to the transition surface, and the ratio of the two horizon radii is much smaller than 1, and depends sensitively on m as shown in Table 2. All these results are significantly different from those obtained in the AOS model.

In review of the results presented in this paper, it is clear that further investigations are highly demanded for LQBH models, in which the two polymerization parameters δ_b and δ_c appearing in Equation (119) are considered Dirac observables of the 4-dimensional phase space, spanned by $(b, p_b; c, p_c)$, before accepting them as viable LQBH models in LQG. In particular, in [49] the consistent gauge-fixing conditions in polymerized gravitational systems were studied, and it would be very interesting to check how these conditions affect the results presented in this paper as well as results obtained in other LQBH models.

Notes-in-addition: When we were finalizing our manuscript, we came across three very interesting and relevant articles [64–66]. We will briefly comment on them here. First, in [64] the authors studied the physical meaning of the three integration constants, C_1, C_2 and $\bar{p}_c^0$, obtained from the integration of the three dynamical equations for the variables c, b and p_c, respectively, and found that C_1 is related to the location of the transition surface, C_2 can be gauged away by the redefinition of time $t \to t + t_0$, where t_0 is a constant, while $\bar{p}_c^0$ is related to the mass parameter. A similar consideration was also carried out in [38] but for the BMM polymer black hole solution [31]. Second, in [65], the authors studied the integrability of $G_b(t_b) \equiv \int_{t_b}^0 F_{cb}(t'_b)dt'_b = \int_{t_c}^0 F_{bc}(t'_c)dt'_c \equiv G_c(t_c)$, the invertibility of $t_i = G_i^{-1}[G_j(t_j)]$, and the overlap of the images of G_i's. It was shown that F_{ij}'s are always integrable so that G_i's always exist. The images of G_i's can be always made overlapped by using the redefinitions of the two time-variables $t'_i = t_i + t_i^0$. In addition, $t_i = G_i^{-1}$ is

always invertible except at the zero points $G_i(t_i^{\rm ext}) = 0$. Moreover, these zero points never correspond to the same moment T, so at least one of the two G_is is invertible at any given moment T. It must be noted that all the studies carried out in [65] were restricted to the internal region. When restricting our studies to this region, our results are consistent with theirs whenever the problems of the integrability, invertibility and overlap of the images, all studied in [65], are concerned. Finally, in [66], the authors considered the quantization of the AOS extended phase space model, and found the conditions that guarantee the existence of physical states in the regime of large black hole masses, among other interesting results.

Author Contributions: All authors contributed equally. All authors have read and agreed to the published version of the manuscript.

Funding: The support provided by the Baylor University High Performance and Research Computing Services for carrying out the numerical computations of this paper. This work is supported in part by the Zhejiang Provincial Natural Science Foundation of China under Grant No. LR21A050001 and LY20A050002, the National Key Research and Development Program of China Grant No.2020YFC2201503, the National Natural Science Foundation of China under Grant No. 11675143 and No. 11975203, and the Fundamental Research Funds for the Provincial Universities of Zhejiang in China under Grant No. RF-A2019015.

Acknowledgments: We would like to thank G.A. Mena Marugán and P. Singh for their valuable discussions, comments and suggestions.

Conflicts of Interest: The authors declare no conflict of interest.

Note

[1] It should be noted that in LQC, there exists only one parameter $\bar{\mu}$ corresponding to the area operator p, and APS set it to $\bar{\mu}^2|p| = \left(4\sqrt{3}\pi\gamma\right)\ell_p^2 \equiv \Delta$ [56], where ℓ_p denotes the Planck scale.

References

1. Ashtekar, A.; Lewandowski, J. Background independent quantum gravity: A Status report. *Class. Quant. Grav.* **2004**, *21*, R53. [CrossRef]
2. Thiemann, T. *Modern Canonical Quantum General Relativity*; Cambridge University Press: Cambridge, UK, 2008.
3. Gambini, R.; Pullin, J. *A First Course in Loop Quantum Gravity*; Oxford University Press: Oxford, UK, 2011.
4. Bojowald, M. *Canonical Gravity and Applications: Cosmology, Black holes, and Quantum Gravity*; Cambridge University Press: Cambridge, UK, 2011.
5. Rovelli, C.; Vidotto, F. *Covariant Loop Quantum Gravity: An Elementary Introduction to Quantum Gravity and SpinFoam Theory*; Cambridge University Press: Cambridge, UK, 2015.
6. Ashtekar, A.; Singh, P. Loop Quantum Cosmology: A Status Report. *Class. Quant. Grav.* **2011**, *28*, 213001. [CrossRef]
7. Ashtekar, A.; Bojowald, M. Quantum geometry and the Schwarzschild singularity. *Class. Quant. Grav.* **2006**, *23*, 391. [CrossRef]
8. Modesto, L. Loop quantum black hole. *Class. Quant. Grav.* **2006**, *23*, 5587. [CrossRef]
9. Böhmer, C.G.; Vandersloot, K. Loop Quantum Dynamics of the Schwarzschild Interior. *Phys. Rev. D* **2007**, *76*, 104030. [CrossRef]
10. Gambini, R.; Pullin, J. Black holes in loop quantum gravity: The Complete space-time. *Phys. Rev. Lett.* **2008**, *101*, 161301. [CrossRef] [PubMed]
11. Campiglia, M.; Gambini, R.; Pullin, J. Loop quantization of spherically symmetric midi-superspaces: The Interior problem. *AIP Conf. Proc.* **2008**, *977*, 52. [CrossRef]
12. Brannlund, J.; Kloster, S.; DeBenedictis, A. The Evolution of Lambda Black Holes in the Mini-Superspace Approximation of Loop Quantum Gravity. *Phys. Rev. D* **2009**, *79*, 084023. [CrossRef]
13. Modesto, L. Semiclassical loop quantum black hole. *Int. J. Theor. Phys.* **2010**, *49*, 1649. [CrossRef]
14. Chiou, D.W. Phenomenological loop quantum geometry of the Schwarzschild black hole. *Phys. Rev. D* **2008**, *78*, 064040. [CrossRef]
15. Chiou, D.W. Phenomenological dynamics of loop quantum cosmology in Kantowski–Sachs spacetime. *Phys. Rev. D* **2008**, *78*, 044019. [CrossRef]
16. Perez, A. The Spin Foam Approach to Quantum Gravity. *Living Rev. Rel.* **2013**, *16*, 3. [CrossRef]
17. Gambini, R.; Pullin, J. Loop Quantization of the Schwarzschild Black Hole. *Phys. Rev. Lett.* **2013**, *110*, 211301. [CrossRef] [PubMed]
18. Gambini, R.; Olmedo, J.; Pullin, J. Quantum black holes in Loop Quantum Gravity. *Class. Quant. Grav.* **2014**, *31*, 095009. [CrossRef]
19. Gambini, R.; Pullin, J. Hawking radiation from a spherical loop quantum gravity black hole. *Class. Quant. Grav.* **2014**, *31*, 115003. [CrossRef]
20. Haggard, H.M.; Rovelli, C. Quantum-gravity effects outside the horizon spark black to white hole tunneling. *Phys. Rev. D* **2015**, *92*, 104020. [CrossRef]

21. Joe, A.; Singh, P. Kantowski–Sachs spacetime in loop quantum cosmology: Bounds on expansion and shear scalars and the viability of quantization prescriptions. *Class. Quant. Grav.* **2015**, *32*, 015009. [CrossRef]
22. Dadhich, N.; Joe, A.; Singh, P. Emergence of the product of constant curvature spaces in loop quantum cosmology. *Class. Quant. Grav.* **2015**, *32*, 185006. [CrossRef]
23. Corichi, A.; Singh, P. Loop quantization of the Schwarzschild interior revisited. *Class. Quant. Grav.* **2016**, *33*, 055006. [CrossRef]
24. Olmedo, J.; Saini, S.; Singh, P. From black holes to white holes: A quantum gravitational, symmetric bounce. *Class. Quant. Grav.* **2017**, *34*, 225011. [CrossRef]
25. Cortez, J.; Cuervo, W.; Morales-Técotl, H.A.; Ruelas, J.C. Effective loop quantum geometry of Schwarzschild interior. *Phys. Rev. D* **2017**, *95*, 064041. [CrossRef]
26. Rovelli, C. Planck stars as observational probes of quantum gravity. *Nature Astron.* **2017**, *1*, 0065. [CrossRef]
27. Perez, A. Black Holes in Loop Quantum Gravity. *Rept. Prog. Phys.* **2017**, *80*, 126901. [CrossRef]
28. Barrau, A.; Martineau, K.; Moulin, F. A status report on the phenomenology of black holes in loop quantum gravity: Evaporation, tunneling to white holes, dark matter and gravitational waves. *Universe* **2018**, *4*, 102. [CrossRef]
29. Rovelli, C.; Martin-Dussaud, P. Interior metric and ray-tracing map in the firework black-to-white hole transition. *Class. Quant. Grav.* **2018**, *35*, 147002. [CrossRef]
30. Bianchi, E.; Christodoulou, M.; D'Ambrosio, F.; Haggard, H.M.; Rovelli, C. White Holes as Remnants: A Surprising Scenario for the End of a Black Hole. *Class. Quant. Grav.* **2018**, *35*, 225003. [CrossRef]
31. Bodendorfer, N.; Mele, F.M.; Münch, J. Effective Quantum Extended Spacetime of Polymer Schwarzschild Black Hole. *Class. Quant. Grav.* **2019**, *36*, 195015. [CrossRef]
32. Martin-Dussaud, P.; Rovelli, C. Evaporating black-to-white hole. *Class. Quant. Grav.* **2019**, *36*, 245002. [CrossRef]
33. Assanioussi, M.; Dapor, A.; Liegener, K. Perspectives on the dynamics in a loop quantum gravity effective description of black hole interiors. *Phys. Rev. D* **2020**, *101*, 026002. [CrossRef]
34. Arruga, D.; Achour, J.B.; Noui, K. Deformed General Relativity and Quantum Black Holes Interior. *Universe* **2020**, *6*, 39. [CrossRef]
35. Ashtekar, A. Black Hole evaporation: A Perspective from Loop Quantum Gravity. *Universe* **2020**, *6*, 21. [CrossRef]
36. Zhang, C.; Ma, Y.; Song, S.; Zhang, X. Loop quantum Schwarzschild interior and black hole remnant. *Phys. Rev. D* **2020**, *102*, 041502. [CrossRef]
37. Gambini, R.; Olmedo, J.; Pullin, J. Spherically symmetric loop quantum gravity: Analysis of improved dynamics. *Class. Quant. Grav.* **2020**, *37*, 205012. [CrossRef]
38. Gan, W.C.; Santos, N.O.; Shu, F.W.; Wang, A. Properties of the spherically symmetric polymer black holes. *Phys. Rev. D* **2020**, *102*, 124030. [CrossRef]
39. Kelly, J.G.; Santacruz, R.; Wilson-Ewing, E. Effective loop quantum gravity framework for vacuum spherically symmetric spacetimes. *Phys. Rev. D* **2020**, *102*, 106024. [CrossRef]
40. Liu, C.; Zhu, T.; Wu, Q.; Jusufi, K.; Jamil, M.; Azreg-Anou, M.; Wang, A. Shadow and Quasinormal Modes of a Rotating Loop Quantum Black Hole. *Phys. Rev. D* **2020**, *101*, 084001. [CrossRef]
41. Bodendorfer, N.; Mele, F.M.; Münch, J. (b,v)-type variables for black to white hole transitions in effective loop quantum gravity. *Phys. Lett. B* **2021**, *819*, 136390. [CrossRef]
42. Giesel, K.; Li, B.F.; Singh, P. Non-singular quantum gravitational dynamics of an LTB dust shell model: The role of quantization prescriptions. *Phys. Rev. D* **2021**, *104*, 106017.
43. Bodendorfer, N.; Mele, F.M.; Münch, J. Mass and Horizon Dirac Observables in Effective Models of Quantum Black-to-White Hole Transition. *Class. Quant. Grav.* **2021**, *38*, 095002. [CrossRef]
44. Sartini, F.; Geiller, M. Quantum dynamics of the black hole interior in loop quantum cosmology. *Phys. Rev. D* **2021**, *103*, 066014. [CrossRef]
45. Li, B.F.; Singh, P. Does the Loop Quantum μ_o Scheme Permit Black Hole Formation? *Universe* **2021**, *7*, 406. [CrossRef]
46. Gambini, R.; Olmedo, J.; Pullin, J. Loop Quantum Black Hole Extensions Within the Improved Dynamics. *Front. Astron. Space Sci.* **2021**, *8*, 74. [CrossRef]
47. Liu, Y.C.; Feng, J.X.; Shu, F.W.; Wang, A. Extended geometry of Gambini-Olmedo-Pullin polymer black hole and its quasinormal spectrum. *Phys. Rev. D* **2021**, *104*, 106001. [CrossRef]
48. Han, M.; Liu, H. Improved effective dynamics of loop-quantum-gravity black hole and Nariai limit. *Class. Quant. Grav.* **2022**, *39*, 035011. [CrossRef]
49. Giesel, K.; Li, B.F.; Singh, P.; Weigl, S.A. Consistent gauge-fixing conditions in polymerized gravitational systems. *Phys. Rev. D* **2022**, *105*, 066023. [CrossRef]
50. Zhang, C.; Ma, Y.; Song, S.; Zhang, X. Loop quantum deparametrized Schwarzschild interior and discrete black hole mass. *Phys. Rev. D* **2022**, *105*, 024069. [CrossRef]
51. Rastgoo, S.; Das, S. Probing the Interior of the Schwarzschild Black Hole Using Congruences: LQG vs. GUP. *Universe* **2022**, *8*, 349. [CrossRef]
52. Gan, W.C.; Ongole, G.; Alesci, E.; An, Y.; Shu, F.W.; Wang, A. Understanding quantum black holes from quantum reduced loop gravity. *arXiv* **2022**, arXiv:2206.07127.
53. Ashtekar, A.; Olmedo, J.; Singh, P. Quantum Transfiguration of Kruskal Black Holes. *Phys. Rev. Lett.* **2018**, *121*, 241301. [CrossRef]
54. Ashtekar, A.; Olmedo, J.; Singh, P. Quantum extension of the Kruskal spacetime. *Phys. Rev. D* **2018**, *98*, 126003. [CrossRef]

55. Ashtekar, A.; Olmedo, J. Properties of a recent quantum extension of the Kruskal geometry. *Int. J. Mod. Phys. D* **2020**, *29*, 2050076. [CrossRef]
56. Ashtekar, A.; Pawlowski, T.; Singh, P. Quantum Nature of the Big Bang: Improved dynamics. *Phys. Rev. D* **2006**, *74*, 084003. [CrossRef]
57. Bouhmadi-López, M.; Brahma, S.; Chen, C.Y.; Chen, P.; Yeom, D.h. Asymptotic non-flatness of an effective black hole model based on loop quantum gravity. *Phys. Dark Univ.* **2020**, *30*, 100701. [CrossRef]
58. Bojowald, M. No-go result for covariance in models of loop quantum gravity. *Phys. Rev. D* **2020**, *102*, 046006. [CrossRef]
59. Bodendorfer, N.; Mele, F.M.; Münch, J. A note on the Hamiltonian as a polymerisation parameter. *Class. Quant. Grav.* **2019**, *36*, 187001. [CrossRef]
60. García-Quismondo, A.; Marugán, G.A.M. Exploring alternatives to the Hamiltonian calculation of the Ashtekar-Olmedo-Singh black hole solution. *Front. Astron. Space Sci.* **2021**, *8*, 701723. [CrossRef]
61. Hawking, S.W.; Ellis, G.F.R. *The Large Scale Structure of Spacetime*; Cambridge University Press: Cambridge, UK, 1973.
62. Barriola, M.; Vilenkin, A. Gravitational Field of a Global Monopole. *Phys. Rev. Lett.* **1989**, *63*, 342. [CrossRef]
63. Martin-Garcia, J.M. xAct: Efficient Tensor Computer Algebra for the Wolfram Language. Available online: http://www.xact.es (accessed on 13 October 2022).
64. Navascués, B.E.; García-Quismondo, A.; Marugán, G.A.M. The space of solutions of the Ashtekar-Olmedo-Singh effective black hole model. *arXiv* **2022**, arXiv:2207.04677.
65. García-Quismondo, A.; Marugán, G.A.M. Two-time alternative to the Ashtekar-Olmedo-Singh black hole interior. *Phys. Rev. D* **2022**, *106*, 023532. [CrossRef]
66. Navascués, B.E.; García-Quismondo, A.; Marugán, G.A.M. Hamiltonian formulation and loop quantization of a recent extension of the Kruskal spacetime. *arXiv* **2022**, arXiv:2208.00425.